

---

# Stable GFlowNets with Probabilistic Guarantees

---

Zengxiang Lei<sup>1</sup> Ananth Shreeekumar<sup>2</sup> Jonathan Rosenthal<sup>2</sup> Ruoyu Song<sup>2</sup> Alvaro A. Cardenas<sup>3</sup>  
Daniel J. Fremont<sup>3</sup> Dongyan Xu<sup>2</sup> Satish Ukkusuri<sup>1</sup> Z. Berkay Celik<sup>2</sup>

## Abstract

Generative Flow Networks (GFlowNets) learn to sample states proportional to an unnormalized reward. Despite their theoretical promise, practical training is often unstable, exhibiting severe loss spikes and mode collapse. To tackle this, we first assess the sensitivity of GFlowNet objectives, demonstrating that a small Total Variation (TV) distance between the learned and target distributions does not preclude an unbounded training loss. Motivated by this mismatch, we establish converse guarantees by deriving loss-to-TV bounds that certify global fidelity from bounded trajectory balance losses. Lastly, we propose an algorithm, *Stable GFlowNets*, that leverages our theoretical results to stabilize training, and empirically demonstrate improved training behavior and superior distributional fidelity.

## 1. Introduction

Generative Flow Networks (GFlowNets) provide a principled framework for learning generative policies to sample states according to a target, unnormalized reward function (Bengio et al., 2021). By modeling generation as a sequential decision process and enforcing flow consistency constraints, GFlowNets enable efficient sampling from complex combinatorial spaces and have shown promise in molecular design, biological sequence discovery, combinatorial optimization, and adversarial generation (Bengio et al., 2021; Jain et al., 2022; Shen et al., 2024; Zhang et al., 2023; Lahlou et al., 2023a).

Despite their successes, training GFlowNets remains challenging in practice. Prior work reports numerical instability (Madan et al., 2025; Malkin et al., 2022a) and difficulty

in reliably capturing rare but high-reward modes (Pan et al., 2023b; Kim et al., 2024c). These behaviors contrast with the comparatively stable and scalable optimization of other likelihood-based generative models (e.g., diffusion models (Rombach et al., 2022)), and raise a fundamental question: *What guarantees on sampling fidelity can we certify with GFlowNet training?*

A central difficulty lies in the ambiguous relationship between non-zero GFlowNet losses and global sampling error. Unlike in reinforcement learning (RL) and diffusion models, where small training loss often yields theoretical guarantees that bound policy performance (Singh & Yee, 1994; Sutton et al., 1998; Song et al., 2021), common GFlowNets training objectives, including flow matching (FM), detailed balance (DB), and trajectory balance (TB), guarantee correctness only at their global optima (i.e., when loss is zero everywhere) (Bengio et al., 2023; Malkin et al., 2022a). In realistic regimes with finite data, function approximation, and non-stationary policies, optimization is necessarily approximate. Furthermore, we demonstrate in Section 3.1 that high loss signals can persist even when the learned policy is near-optimal. Consequently, it is unclear whether observed loss values meaningfully reflect distributional fidelity, or whether controlling the loss is sufficient to bound the mismatch between the learned state distribution and the target reward distribution.

In this work, we close this gap by establishing a rigorous connection between GFlowNet training losses and the global Total Variation (TV) error, i.e., the total variation distance between the learned distribution and the reward-proportional target. We show, in an analytically tractable setting, that **small TV error does not imply bounded training loss**, so extreme optimization signals may arise even when the learned distribution is globally accurate. We then derive loss-to-TV bounds that certify global fidelity from bounded TB losses, and we further provide finite-sample TV certificates via trajectory sampling. Since loss spikes can be inevitable, we analyze *reference flow*, a customized flow injected into the flow conservation constraints to prevent extreme ratios and thus cap GFlowNet loss, as a stabilization mechanism that reduces loss magnitudes without altering the global objective, and quantify the resulting stability-fidelity trade-off. Building on these insights, we propose *Stable GFlowNets*,

<sup>1</sup>Lyles School of Civil and Construction Engineering, Purdue University, IN, USA <sup>2</sup>Department of Computer Science, Purdue University, IN, USA <sup>3</sup>Computer Science and Engineering, University of California, Santa Cruz, USA. Correspondence to: Z. Berkay Celik <zcelik@purdue.edu>, Satish Ukkusuri <sukkusur@purdue.edu>.

which uses adaptive reference flows to stabilize incremental learning and certify global performance. Our contributions are summarized as follows:

1. We characterize the sensitivity of GFlowNet objectives and prove that a low Total Variation (TV) error does not imply bounded training loss.
2. We derive the first series of loss-to-TV bounds connecting GFlowNet training losses to fidelity of the learned distribution to the target.
3. We introduce *Stable GFlowNets*, which stabilizes GFlowNets training via adaptive reference flow, and demonstrate improved stability and mode coverage.

## 2. Preliminaries

**Notation.** We consider a finite directed acyclic graph (DAG)  $\mathcal{G} = (\mathcal{S}, \mathcal{A})$  where the set of nodes forms the state space  $\mathcal{S}$  and the set of directed edges forms the action space  $\mathcal{A}$ . The unique state with no incoming edges is the initial state  $s_0 \in \mathcal{S}$ , and the unique state with no outgoing edges is the final state  $s_f \in \mathcal{S}$ . States that transition only to  $s_f$  are referred to as terminating (or end) states; their set is denoted by  $\mathcal{X} \subseteq \mathcal{S}$ . A (complete) trajectory is defined as a sequence of states  $\tau = (s_0 \rightarrow \dots \rightarrow s_n \rightarrow s_{n+1} = s_f)$  where the terminating state  $s_n \in \mathcal{X}$  and each action (or edge)  $s_i \rightarrow s_{i+1} \in \mathcal{A}$ . In contrast, any prefix of such a sequence is a subtrajectory. The set of all complete trajectories is denoted by  $\mathcal{T}$ . Each trajectory  $\tau$  is assigned a positive flow value  $F_{traj} : \tau \rightarrow \mathbb{R}_+$ , which induces state-level flow and edge-level flow as  $F_{state}(s) = \sum_{\tau \in \mathcal{T}, s \in \tau} F_{traj}(\tau)$  and  $F_{edge}(s, s') = \sum_{\tau \in \mathcal{T}, s \rightarrow s' \in \tau} F_{traj}(\tau)$ , respectively. Each edge is further evaluated by a forward policy  $P_F : \mathcal{S} \times \mathcal{S} \rightarrow (0, 1)$  and a backward policy  $P_B : \mathcal{S} \times \mathcal{S} \rightarrow (0, 1)$ ; when evaluated on a specific edge  $s \rightarrow s'$ , they define the transition probability  $P_F(s, s') = P(s' | s)$  and  $P_B(s, s') = P(s | s')$ . A positive scalar  $Z$  (the partition function, if treated as learnable) relates flow to policy via  $F_{traj}(\tau) = ZP_F(\tau) = Z\prod_{t=0}^n P_F(s_t, s_{t+1})$ , and we have the marginal distribution of the flow over terminating states  $\mathcal{X}$  as  $P_T(x) = F_{state}(x)/Z$ . The reward satisfies  $R(s) > 0$  for all  $s \in \mathcal{X}$  and  $R(s) = 0$  for  $s \notin \mathcal{X}$ .

**GFlowNets.** Depending on the specific parameterization, GFlowNets learn either an edge flow  $F_{edge}$  or a state flow  $F_{state}$  (or a partition function  $Z$ ) along with a forward policy  $P_F$  (and optionally with a backward policy  $P_B$ ). The training objectives ensure that the generated flow on the DAG  $\mathcal{G}$  results in a sampling probability proportional to the reward,  $F_{state}(x) \propto R(x)$  for all  $x \in \mathcal{X}$ . The backward policy is optional because the GFlowNet framework permits  $P_B$  to be chosen arbitrarily (Bengio et al., 2023). However,

fixing  $P_B$  constrains the forward policy  $P_F$  to a unique solution, whereas learning  $P_B$  jointly with  $P_F$  can empirically accelerate convergence (Malkin et al., 2022a). The choice between learning  $F_{state}$  versus learning  $Z$  depends on the training objective: objectives such as trajectory balance estimate  $Z$  jointly with  $P_F$ , while others learn flows  $F_{state}$  and take  $Z = F_{state}(s_0)$  implicitly. Given the terminating state space  $\mathcal{X}$ , the true partition function  $Z^*$  can be computed explicitly as  $Z^* = \sum_{x \in \mathcal{X}} R(x)$  and the ground-truth target distribution is  $\pi_{target}(x) = \frac{R(x)}{Z^*}$ ; however, GFlowNets are primarily motivated by settings where  $|\mathcal{X}|$  is exponentially or combinatorially large, making such aggregation intractable.

**Training objectives.** GFlowNets can be trained using several objectives that enforce the global flow-matching condition  $F(x) \propto R(x)$  through different forms of local consistency. These objectives differ in where the consistency constraint is localized: on individual edges, on flow conservation at states, or on trajectories.

- **Flow matching (FM).** Bengio et al. (2021) enforces flow conservation at each intermediate state:

$$\mathcal{L}_{FM}(s') = \left( \log \frac{\sum_{s \rightarrow s' \in \mathcal{A}} F_{edge}(s, s')}{R(s') + \sum_{s' \rightarrow s'' \in \mathcal{A}, s'' \neq s_f} F_{edge}(s', s'')} \right)^2 \quad (1)$$

In Bengio et al. (2021), a hyperparameter  $\delta$  was introduced to mitigate numerical issues. For simplicity in our theoretical analysis, we omit  $\delta$  here and discuss its role in Section 4.

- **Detailed balance (DB).** Bengio et al. (2023) enforces local consistency on individual edges by equating forward and backward flows:

$$\mathcal{L}_{DB}(s, s') = \left( \log \frac{F_{state}(s)P_F(s, s')}{F_{state}(s')P_B(s, s')} \right)^2 \quad (2)$$

where  $s \rightarrow s' \in \mathcal{A}$ ,  $s' \neq s_f$ , and  $F_{state}(s') := R(x)$  when  $s' = x \in \mathcal{X}$ .

- **Trajectory balance (TB).** Malkin et al. (2022a) imposes consistency on complete trajectories  $\tau = (s_1 \rightarrow s_2 \rightarrow \dots \rightarrow s_n = x \rightarrow s_f)$ :

$$\mathcal{L}_{TB}(\tau) = \left( \log \frac{Z\prod_{t=0}^{n-1} P_F(s_t, s_{t+1})}{R(x)\prod_{t=0}^{n-1} P_B(s_t, s_{t+1})} \right)^2 \quad (3)$$

- **Subtrajectory balance (subTB).** Pan et al. (2023a) extends TB to subtrajectories  $\tau^{patial} = (s_{t_1} \rightarrow \dots \rightarrow$

$$\begin{aligned}
 & s_{t_2}): \\
 & \mathcal{L}_{\text{subTB}}(\tau_{t_1:t_2}) \\
 & = \left( \log \frac{F_{\text{state}}(s_{t_1}) \prod_{t=t_1}^{t_2-1} P_F(s_t, s_{t+1})}{F_{\text{state}}(s_{t_2}) \prod_{t=t_1}^{t_2-1} P_B(s_t, s_{t+1})} \right)^2 \quad (4)
 \end{aligned}$$

where  $F_{\text{state}}(s_{t_2}) := R(x)$  when  $s_{t_2} = x \in \mathcal{X}$ .

**Total Variation (TV) Error.** Total Variation (TV) error quantifies the distributional discrepancy and is central to recent theoretical analyses of GFlowNets (Silva et al., 2025). The TV error corresponds to half the total  $L_1$  error:

$$TV(P_T, \pi_{\text{target}}) = \frac{1}{2} \sum_{x \in \mathcal{X}} |P_T(x) - \pi_{\text{target}}(x)| \quad (5)$$

### 3. On the Sensitivity and Fidelity of GFlowNets

Our analysis is motivated by the challenge of incremental mode coverage, where a GFlowNet must progressively incorporate new high-reward modes into its sampling distribution without suffering from catastrophic forgetting. In Section 3.1, we demonstrate that standard GFlowNet objectives are ill-conditioned for this task, as arbitrarily small perturbations in the target distribution can trigger unbounded local losses driven by worst-case local contrast ratios (the maximum local ratio between the target mass and the model-implied mass appearing in the objective). This motivates the reverse question of how much fidelity can be guaranteed when training losses are controllably bounded. Section 3.2 answers this by deriving bounds linking training loss to TV error (Theorem 3.5) and provides a practical probabilistic certificate via trajectory sampling (Theorem 3.6). We subsequently introduce reference flow in Section 3.3 to stabilize training by smoothing local contrast; while this effectively caps loss magnitudes, we prove it imposes an inherent fidelity trade-off: a multiplicative fidelity degradation governed by the augmentation magnitude (Theorem 3.10). We conclude by deriving a probabilistic certificate for reference-flow-stabilized GFlowNets (Theorem 3.11), which directly informs the training procedure in Section 3.4.

#### 3.1. Incremental Mode Coverage Causes Loss Explosion

To lay the groundwork, we examine the simplified setting in Figure 1. The following remarks illustrate a sharp mismatch between global flow error and local training behavior. Remark 3.1 shows that adding a reward to a single leaf in a large tree ( $g^h$  leaves) results in a negligible Total Variation error of  $TV(P_T, \pi_{\text{target}}) \approx 1/g^h$ . However, Remark 3.2 reveals that the local loss scales as  $(\log \epsilon)^2$ . As  $\epsilon \rightarrow 0$ , the training loss diverges to  $+\infty$ , even though the global distribution is nearly correct.

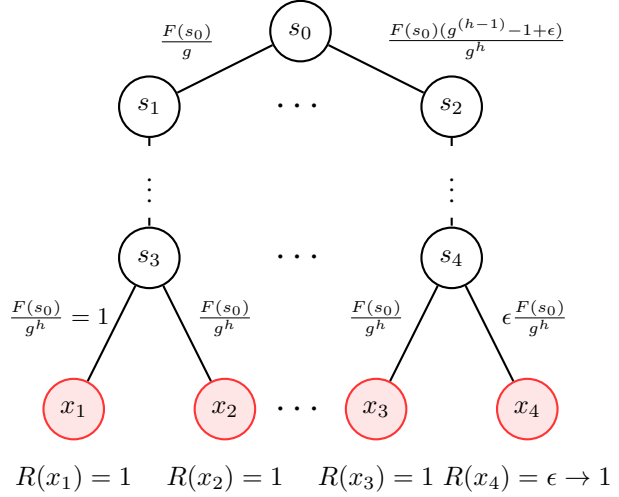


Figure 1. The “one more mode” learning setup on a  $g$ -ary tree of depth  $h$ . The underlying structure is a regular tree. We initialize the experiment with an already fitted model where this specific node leads to a negligible reward  $R(x_4) = \epsilon (\ll 1)$ . To introduce the new mode, we update the reward function by promoting  $x_4$  to a high-reward state with  $R(x_4) = 1$ . The objective is to learn this new mode while preserving the previously acquired ones.

**Remark 3.1.** Flow error for “one more mode” learning over a regular tree.

$$\begin{aligned}
 & TV(P_F, \pi_{\text{target}}) \\
 & = \frac{(g^h - 1)}{2} \left( \frac{1}{g^h - 1 + \epsilon} - \frac{1}{g^h} \right) + \frac{1}{2} \left( \frac{1}{g^h} - \frac{\epsilon}{g^h - 1 + \epsilon} \right) \\
 & \approx \frac{1}{g^h} \quad (6)
 \end{aligned}$$

**Remark 3.2.** Training loss for “one more mode” learning over a regular tree.

Most losses are zero; non-zero losses are shown below and are all  $(\log \epsilon)^2$ .

$$\begin{aligned}
 \mathcal{L}_{FM}(x_4) & = \mathcal{L}_{DB}(s_4, x_4) = \mathcal{L}_{TB}(\tau \ni x_4) \\
 & = \mathcal{L}_{\text{subTB}}(\tau^{\text{partial}} \ni x_4) = (\log \epsilon)^2 \quad (7)
 \end{aligned}$$

This implies that the GFlowNet training signal does not necessarily reflect the scale of the distributional mismatch. Instead, it can be dominated by worst-case local contrast ratios (i.e., states where the learned flow is orders of magnitude smaller than what the target implies).

For a general **incremental mode coverage** setting, we assume that the network has converged to an initial reward landscape  $R_{\text{prev}}(x)$  such that  $F_{\text{state}}(x) = R_{\text{prev}}(x)$ , and we are introducing a new reward  $R_{\text{new}}(x) = R_{\text{prev}}(x) + R'(x)$  where  $R'(x) \geq 0$ .

**Proposition 3.3.** (TV bound for incremental mode coverage over arbitrary state graph). Let the reward added at each state in a subset  $\mathcal{X}_{sub}$  be  $R'(x)$ . We define the local true partition function  $Z_{\mathcal{Y} \subseteq \mathcal{X}}^* = \sum_{x \in \mathcal{Y}} R(x)$  and the local contrast ratio  $\Lambda_{\mathcal{Y}} = \frac{Z_{\mathcal{Y}}^*}{Z_{\mathcal{Y}^* + \sum_{x \in \mathcal{Y}} R'(x)}}$ . Then, we have

$$\frac{Z^* - Z_{\mathcal{X}_{sub}}^*}{Z^*} (1 - \Lambda_{\mathcal{X}}) \leq TV(P_T, \pi_{target}) \leq (1 - \Lambda_{\mathcal{X}}) \quad (8)$$

Here, note that  $Z^* = Z_{\mathcal{X}}^*$  is the true partition function on the original reward function.

**Proposition 3.4.** (Loss scale via local contrast). While the TV error depends on the aggregate  $\Lambda_{\mathcal{X}}$ , the supremum of the training loss is governed by the **worst-case** local contrast ratio, given by:

$$\sup |\mathcal{L}_{GFN}| = \left( \log \min_{\{x\} \subseteq \mathcal{X}_{sub}} \Lambda_{\{x\}} \right)^2 \quad (9)$$

where  $GFN \in \{FM, DB, TB, subTB\}$ .

n

Proofs of Proposition 3.3 and 3.4 are given in Appendix A. Taken together, the propositions show that the incremental mode coverage in GFlowNets is characterized by two distinct quantities. On one hand, the global TV error is controlled by aggregate contrast ratios such as  $1 - \Lambda_{\mathcal{X}}$ , which can remain small when the new mode only occupies a tiny portion of the reward mass. On the other hand, the worst-case local contrast ratio  $\min_{\{x\} \subseteq \mathcal{X}_{sub}} \Lambda_{\{x\}}$  drives the scale of both the loss and the gradients through terms of the form  $(\log \min_{\{x\}} \Lambda_{\{x\}})^2$ . When the new mode demands a large relative increase in reward at previously rarely visited states, these local contrast ratios become extremely small, and the training dynamics degenerate into a regime where tiny changes in the target distribution cause huge optimization signals.

### 3.2. The General Link Between GFlowNets Training Loss and TV Error

As TV error does not effectively bound GFlowNet training losses, we pursue the reverse direction to bound the TV error of the resulting policy if the training loss can be contained, yielding the following theorems for the general setting.

**Theorem 3.5.** (Training loss to TV distance bound). The relationship between the training loss bound and the resulting TV distance depends on the scope of the objective (trajectory-level vs. transition-level):

**Trajectory-level Objective.** If the trajectory loss is bounded, i.e.,  $\mathcal{L}_{TB}(\tau) \leq c^2, \forall \tau \in \mathcal{T}$ , the TV error is bounded by:

$$TV(P_T, \pi_{target}) \leq 1 - \exp(-2c) \quad (10)$$

This bound is independent of the trajectory length, as TB optimizes the full path consistency directly.

**Transition-level Objective.** If the local transition loss is bounded, i.e.,  $\mathcal{L}_{DB}(s, s') \leq c^2$  or  $\mathcal{L}_{FM}(s') \leq c^2$ , the global consistency relies on the accumulation of local estimates. For trajectories of maximum length  $L$ , the error bound degrades linearly with depth in the log-domain:

$$TV(P_T, \pi_{target}) \leq 1 - \exp(-2Lc) \quad (11)$$

Since DB and FM bounds depend on the maximum trajectory length, we focus our analysis on the TB loss. Extensions to the DB and FM cases follow directly by introducing the trajectory length into the bounds. The proof can be found in Appendix A.

As verifying the loss  $\mathcal{L}_{TB} \leq c^2$  for each trajectory is intractable, we develop a probabilistic certificate using random sampling. It is worth noting that this certificate is independent of the size of the state space.

**Theorem 3.6.** (Probabilistic TV bound via trajectory sampling). Given the ground-truth target distribution  $\pi_{target}$ , we define a target distribution over trajectories  $\hat{\pi}(\tau) = \pi_{target}(x_\tau) P_B(\tau | x_\tau)$ . Sample  $m$  trajectories  $\tau_1, \dots, \tau_m$  from  $\hat{\pi}$  independently by sampling  $x \sim \pi_{target}$  and  $\tau \sim P_B(\cdot | x)$ . Sample another  $n$  trajectories independently using  $P_F$ . Suppose we observe  $\mathcal{L}_{TB}(\tau_i) \leq c^2$  for all trajectories in both sets. With confidence  $1 - 2\alpha$ , the global TV error is bounded by:

$$TV(P_T, \pi_{target}) \leq \exp(2c) - 1 + \frac{\log(1/\alpha)}{m} + \frac{\log(1/\alpha)}{n} \quad (12)$$

The proof is provided in Appendix A. When sampling end states from the full ground-truth target distribution is replaced by sampling from a subset  $\mathcal{X}_{sub} \subseteq \mathcal{X}$ , the theorem yields a *subgraph certificate* over  $\mathcal{X}_{sub}$ .

**Corollary 3.7.** (Subgraph Certification via trajectory sampling). Let  $\mathcal{X}_{sub} \subseteq \mathcal{X}$  be a subset of end-states. Define the restricted target distribution over  $\mathcal{X}_{sub}$  by  $\pi_{target}^{sub}(x) = \frac{\sum_{x \in \mathcal{X}_{sub}} R(x)}{\sum_{x \in \mathcal{X}} R(x)}$ , the corresponding restricted target trajectory distribution as  $\hat{\pi}_{sub}(\tau) = \pi_{target}^{sub}(x_\tau) P_B(\tau | x_\tau)$ . Sample  $m$  trajectories  $\tau_1, \dots, \tau_m$  from  $\hat{\pi}_{sub}$ . Sample another  $n$  trajectories that end within  $\mathcal{X}_{sub}$  independently using  $P_F$ . Suppose we observe  $\mathcal{L}_{TB}(\tau_i) \leq c^2$  for all trajectories in both sets. Let  $P_T^{sub}$  denote the terminal flow  $P_T$  renormalized to  $\mathcal{X}_{sub}$ . Then, with confidence  $1 - 2\alpha$ ,

$$TV(P_T^{sub}, \pi_{target}^{sub}) \leq \exp(2c) - 1 + \frac{\log(1/\alpha)}{m} + \frac{\log(1/\alpha)}{n} \quad (13)$$

If  $\mathcal{X}_{sub}$  dominates the total reward mass and the estimated

partition function  $Z$  matches this captured mass, i.e.,

$$\sum_{x \in \mathcal{X} \setminus \mathcal{X}_{\text{sub}}} R(x) \ll \sum_{x \in \mathcal{X}_{\text{sub}}} R(x) \quad , \quad Z \approx \sum_{x \in \mathcal{X}_{\text{sub}}} R(x), \quad (14)$$

then the certified model is near-optimal (up to total variation error provided in Equation (13) globally with high probability. This follows by extending the subgraph-level guarantee to the full space via the above conditions.

### 3.3. Reference Flow: Stability with Fidelity Trade-off

The bounds in Section 3.2 are only useful if the training loss can be kept small, a requirement that could be easily violated as seen in Section 3.1. To resolve this, we investigate **reference flow**, which artificially increases the background flow to reduce the training losses.

**Definition 3.8.** (Trajectory reference flow). For a trajectory  $\tau$ , let  $\mathcal{R}(\tau) = R(x)P_B(\tau|x)$  be the target flow. We introduce a trajectory-specific, non-negative reference flow  $\delta(\tau) > 0$  to augment the existing one. The augmented flow  $F_{\text{aug}}(\tau)$  and augmented target  $\mathcal{R}_{\text{aug}}(\tau)$  are defined as:  $F_{\text{aug}}(\tau) = ZP_F(\tau) + \delta(\tau)$ ,  $\mathcal{R}_{\text{aug}}(\tau) = \mathcal{R}(\tau) + \delta(\tau)$

*Remark 3.9.* (Stabilization via reference flow). Let  $\mathcal{L}_{\text{TB}}(\tau) = \left(\log \frac{ZP_F(\tau)}{\mathcal{R}(\tau)}\right)^2$  be the standard TB loss. The reference flow objective reduces the scale of the TB loss:

$$\mathcal{L}_{\text{aug}}(\tau) = \left(\log \frac{F_{\text{aug}}(\tau)}{\mathcal{R}_{\text{aug}}(\tau)}\right)^2 = \frac{1}{\gamma^2} \mathcal{L}_{\text{TB}}(\tau) \quad (15)$$

where the reduction factor  $\gamma$  is given by:

$$\gamma = 1 + \log \left( 1 + \frac{\frac{ZP_F(\tau)}{\mathcal{R}(\tau)} - 1}{\frac{ZP_F(\tau)}{\mathcal{R}(\tau)} + 1} \right) / \log \left( \frac{ZP_F(\tau) + \delta(\tau)}{\mathcal{R}(\tau) + \delta(\tau)} \right) \quad (16)$$

It is easy to verify that  $\gamma > 1$ , and to make  $\mathcal{L}_{\text{aug}}(\tau) \leq c^2$ , we have the minimum reference flow satisfying:

$$\delta(\tau) = \begin{cases} \frac{ZP_F(\tau) - \exp(c)\mathcal{R}(\tau)}{\exp(c) - 1} & \text{if } \log \frac{ZP_F(\tau)}{\mathcal{R}(\tau)} > c \\ \frac{\mathcal{R}(\tau) - \exp(c)ZP_F(\tau)}{\exp(c) - 1} & \text{if } \log \frac{ZP_F(\tau)}{\mathcal{R}(\tau)} < -c \\ 0 & \text{otherwise} \end{cases} \quad (17)$$

We note that adding reference flow can be viewed as a pre-defined modification of the target distribution, which makes the resulting model amenable to analysis via Theorem 3.5. This perspective makes the trade-off explicit:

**Theorem 3.10.** (Fidelity trade-off under reference flow).

*The fidelity of the recovered policy depends on the ratio between the training loss and the augmentation magnitude. Let the total reference flow be  $\Delta = \sum_{\tau \in \mathcal{T}} \delta(\tau)$ . If the*

*reference training loss is bounded by  $\mathcal{L}_{\text{aug}}(\tau) \leq c^2$ , the TV error of the learned flow  $P_F$  is bounded by:*

$$\text{TV}(P_T, \pi_{\text{target}}) \leq (1 - \exp(-2c))(1 + \frac{\Delta}{Z^*}) \quad (18)$$

We observe that the ratio  $\frac{\Delta}{Z^*}$  can be expressed as the expectation of  $\frac{\delta(\tau)}{\mathcal{R}(\tau)}$  over the target distribution  $\hat{\pi}(\tau) = \frac{\mathcal{R}(\tau)}{Z^*}$ . **This provides a practical approach to approximate the TV bound via Monte Carlo estimation.** Furthermore, this insight yields a probabilistic bound that is consistently tighter than the loss-based result in Theorem 3.6.

**Theorem 3.11.** (Probabilistic TV bound of reference flow).

*Sample  $m$  trajectories  $\tau_1, \dots, \tau_m$  independently from the target  $\hat{\pi}$ , sample another  $n$  trajectories  $\tau_{m+1}, \dots, \tau_{m+n}$  independently using  $P_F$ , we compute the reference flow  $\delta(\tau_i)$  required to bound the reference loss by  $c^2$  according to Equation (17). When  $M := \max_{i \in \{1, \dots, m+n\}} \frac{\delta(\tau_i)}{\mathcal{R}(\tau_i)} < \frac{1}{\exp(c) - 1}$ , with confidence  $1 - 2\alpha$ , the global TV error is bounded by:*

$$\text{TV}(P_T, \pi_{\text{target}}) \leq \frac{\log(1/\alpha)}{m} + \frac{\log(1/\alpha)}{n} + \left( \frac{\exp(c) + (\exp(c) - 1)M}{\exp(-c) - (1 - \exp(-c))M} - 1 \right) \quad (19)$$

For fixed  $c$ , the bound in Equation (19) is monotonically increasing in  $M$ . In particular, when  $M = 0$ , this bound reduces exactly to Equation (12). Similar to Corollary 3.7, when sampling from the ground truth  $\hat{\pi}$  is replaced with sampling from  $\hat{\pi}_{\text{sub}}$ , the resulting certificate is correspondingly restricted to  $\mathcal{X}_{\text{sub}}$ .

### 3.4. Applications to GFlowNets Training

Theorem 3.11 motivates a practical training procedure (Algorithm 1): we adaptively inject a reference flow  $\delta(\tau)$  based on the instantaneous mismatch and monitor the resulting probabilistic global/subgraph-level TV certificate. When the terminating-state space  $\mathcal{X}$  is intractable to support exact backward sampling, we restrict certification to a subgraph  $\mathcal{X}_{\text{sub}} \subset \mathcal{X}$ , implemented as a buffer of discovered top- $K$  high-reward end states. In typical GFlowNet applications,  $K$  can be chosen modestly while still capturing most of the reward mass.

Algorithm 1 shows the principles of *Stable GFlowNets*. We now describe (1) how we choose/update the loss threshold  $c$ , and (2) how we compute the probabilistic TV bound  $\mathcal{B}_{\text{TV}}$  (and similarly the estimated TV bound derived from Theorem 3.10).

**Adaptive threshold selection.** The loss threshold  $c$  controls the extent of stabilization by capping the effective

training loss. Since the typical scale of  $\mathcal{L}_{TB}$  is problem-dependent (e.g., reward scale, environment size, and policy entropy), a fixed global choice is brittle. We therefore treat  $c$  as an adaptive parameter and update it online using an exponential moving-average rule, analogous to the soft target updates used in reinforcement learning (Lillicrap et al., 2015). Concretely, at iteration  $t$ , we set

$$c_{t+1} \leftarrow (1 - \beta) c_t + \beta \max_{\tau \in \mathcal{T}_{batch}} \sqrt{\mathcal{L}_{TB}(\tau)}, \quad (20)$$

where  $\beta \in (0, 1)$  is a small smoothing coefficient (we use  $\beta = 0.05$  for our experiments). This update tracks the prevailing loss scale while avoiding abrupt changes, ensuring that stabilization remains neither overly conservative (too small  $c$ ) nor inactive (too large  $c$ ). The aggregation operator is chosen heuristically, and Appendix D.2 compares max, mean, and median aggregations empirically.

**Computing  $\mathcal{B}_{TV}$  via 1D optimization.** We compute the probabilistic certificate  $\mathcal{B}_{TV}$  (and similarly the estimated TV bound from Theorem 3.10) by exploiting a one-dimensional structure. For a fixed threshold  $c$ , the bound is monotone in the reference-flow magnitude, so tightening the certificate reduces to a bounded scalar optimization over that single degree of freedom. In practice, we use `scipy.optimize.minimize_scalar` with a bounded search interval. The interval’s upper bound is  $\max_i \mathcal{L}_{TB}(\tau_i)$ , the lower bound is obtained from Equation (17) and the condition  $\frac{\delta(\tau)}{\mathcal{R}(\tau)} < \frac{1}{\exp(c)-1}$ :

$$c > \begin{cases} \log \left( \frac{Z P_F(\tau)}{\mathcal{R}(\tau)} - 1 \right), & \text{if } \frac{Z P_F(\tau)}{\mathcal{R}(\tau)} > 1 \\ \log \left( \frac{\mathcal{R}(\tau)}{Z P_F(\tau)} - 1 \right), & \text{if } \frac{Z P_F(\tau)}{\mathcal{R}(\tau)} < 1 \end{cases} \quad (21)$$

## 4. Related Work

**Theoretical Analysis of GFlowNets.** The theoretical foundations of GFlowNets have evolved substantially since their introduction as a flow-matching framework on directed acyclic graphs (Bengio et al., 2023). The development of the Trajectory Balance (TB) loss (Malkin et al., 2022a) addressed long-horizon credit assignment and established a stable training objective. Subsequent work connected GFlowNets to broader generative and control paradigms, including continuous-space extensions and links to diffusion models (Lahlou et al., 2023a), variational inference (Malkin et al., 2022b), and entropy-regularized reinforcement learning (Tiapkin et al., 2024). Recent theoretical work characterized how flow perturbations translate to TV error and revealed inherent identifiability limits in GNN-based GFlowNets (Silva et al., 2025).

Building on this line of work, we advance GFlowNet theory in three ways: (1) we derive explicit bounds linking

---

### Algorithm 1 Stable GFlowNets with Prob. Guarantees

---

**Require:** TV target  $d$ ; confidence  $1 - 2\alpha$ ; loss threshold  $c$ ; patience  $N$

- 1: Initialize probabilistic TV bound  $\mathcal{B}_{TV} \leftarrow 1$ , high-reward end states  $\mathcal{X}_{sub} \leftarrow \emptyset$ , patience counter  $n \leftarrow 0$
  - 2: **while**  $\mathcal{B}_{TV} > d$  and maximum rounds not reached **do**
  - 3:   Sample a batch of trajectories  $\mathcal{T}_{batch}$  from  $P_F$  and via backward sampling: draw  $x \in \mathcal{X}_{sub}$  with probability  $\propto R(x)$ , then sample  $\tau \sim P_B(\cdot|x)$ ;
  - 4:   Update  $\mathcal{X}_{sub}$  by retaining the top- $K$  highest reward states from  $\mathcal{X}_{sub} \cup \{s \mid s \in \tau, \forall \tau \in \mathcal{T}_{batch}\}$ ;
  - 5:    $n \leftarrow \mathbb{I}\{\mathcal{X}_{sub} \text{ unchanged}\} (n + 1)$
  - 6:   **if**  $n \geq N$  **then**
  - 7:     Compute  $\mathcal{B}_{TV}$  via Theorem 3.11 restricted to trajectories terminating in  $\mathcal{X}_{sub}$ ;
  - 8:   **end if**
  - 9:   **if** the first term in  $\mathcal{B}_{TV}$ ’s Equation (19)  $< d$  **then**
  - 10:     Skip training to accumulate samples
  - 11:   **else**
  - 12:     Compute reference flow via Equation (17)
  - 13:     Update  $P_F, P_B, \log Z$  via  $\mathcal{L}_{aug}$
  - 14:   **end if**
  - 15: **end while**
  - 16: **return**  $P_F, P_B, \log Z, \mathcal{B}_{TV}, \mathcal{X}_{sub}$
- 

GFlowNets training loss to TV distance; (2) we strengthen this result with a practical probabilistic performance guarantee; and (3) we use this framework to characterize the stability-fidelity trade-offs imposed by reference flows.

**Theoretical Analysis of RL and Diffusion.** It is well-established in these related domains that a bounded training objective translates directly to theoretical performance guarantees under mild assumptions. In RL, bounds on value-function error yield performance bounds for the corresponding greedy policy (Singh & Yee, 1994), whereas inaccurate advantage estimates can invalidate monotonic-improvement guarantees and lead to policy degradation (Schulman et al., 2015). In diffusion models, the training loss upper-bounds the negative log-likelihood under the data distribution (Song et al., 2021). GFlowNets combine distribution matching (as in diffusion) with active exploration for high-reward states (as in RL), yet differ from both: they train without a fixed dataset and optimize distributional fidelity rather than reward maximization. This makes it nontrivial to determine when training-time samples faithfully represent global objectives, which we address in our probabilistic certifications.

**GFlowNets Training.** Here, we focus on prior methods most relevant to the development of our stable GFlowNets algorithm. A broader discussion connecting empirical observations in the literature to our theoretical analysis is deferred to Appendix B.

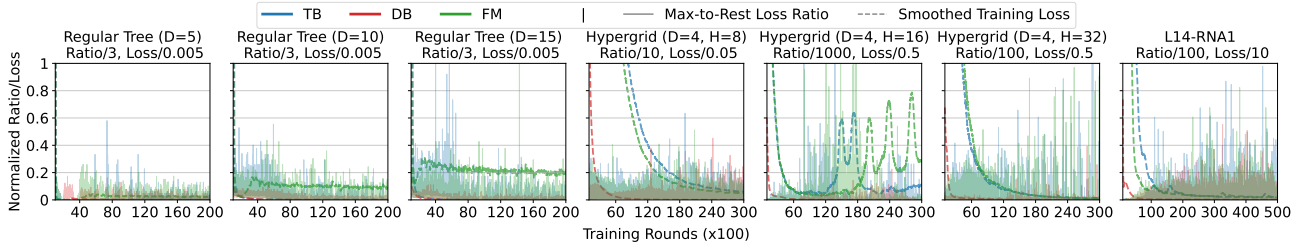


Figure 2. Loss Concentration and Training Stability. Solid lines (left axis) show the Max-to-Rest Loss Ratio, defined as  $\frac{\max_i \mathcal{L}_{TB}(\tau_i)}{\sum_{j \neq i} \mathcal{L}_{TB}(\tau_j)}$ , and dashed lines (right axis) show the smoothed training loss (time window = 1000). Spikes in the ratio indicate outlier-dominated updates and serve as a proxy for training instability. We note the largest spikes occur at Hypergrid  $H = 16$ ; at  $H = 32$ , TB/FM rarely sample trajectories from different reward clusters, reducing observed spikes (Appendix D).

Numerical instability is a persistent challenge in training GFlowNets. Common remedies include adding a small constant  $\delta$  to transitional flows (Bengio et al., 2021; 2023), clipping the maximum loss (Lahlou et al., 2023b) or the gradient norm (Shen et al., 2023). While introducing a fixed  $\delta$  can improve numerical stability, Theorem 3.10 shows that it induces a resolution loss in the resulting TV guarantee. Even when  $\delta$  is chosen as the smallest attainable reward, this resolution loss can lead to vacuous guarantees and may still be insufficient to stabilize training in practice. Loss or gradient clamping, although empirically effective, does not generally correspond to a bounded loss certificate, thus disconnecting from formal guarantees.

Efficient exploration is essential for GFlowNet training. Besides annealing the scale of  $\log P_F$  to promote uniform sampling behavior (Lahlou et al., 2023b). Generative Augmented Flow Networks (GAFN) (Pan et al., 2023b) introduce stochastic transition augmentations to encourage visits to underexplored regions of the state space. Local search GFlowNets (Kim et al., 2024c) perform a backtrack-and-reconstruct procedure: they backtrack from a forward-generated complete trajectory using the backward policy and then roll forward from an intermediate state to propose alternative completions, enabling localized exploration around previously discovered modes. A more recent work is Adaptive Teacher (Kim et al., 2025b), which leverages a teacher policy to focus sampling on high-loss regions of the student policy. We contribute by reframing exploration as a mechanism for certification, not just heuristic mode discovery. In particular, we show that backward trajectories sampled from the reward distribution and  $P_B$  enable a theoretical bound on the global total variation (TV) error, highlighting the need to discover and adequately visit these states and trajectories.

## 5. Experiments

To evaluate the practical implications of our theory and the effectiveness of Stable GFlowNets, we conduct experiments

Table 1. Overview of the experimental design, mapping research questions (RQs) to specific environments, metrics, and baselines.

RQ	Environments	Metrics	Algorithms
RQ1	All	Training Loss	DB/FM/TB
RQ2	Hypergrid, L14-RNA1	Total $L_1$ error/ # modes	DB/FM/TB/SubTB/ WDB/Teacher/Stable
RQ3	All	True TV/ Total $L_1$ Error/ TV bounds	Stable (Ours)

designed to address three core questions: (1) **RQ1**: To what extent do loss instabilities manifest in general GFlowNets training? (2) **RQ2**: Does the proposed stable GFlowNet improve training stability, convergence speed, and mode coverage? (3) **RQ3**: How are Theorem 3.10 and Theorem 3.11 reflected in practice?

### 5.1. Experimental Setup

#### 5.1.1. ENVIRONMENTS.

**Regular Tree** is a 3-ary tree of depth  $D$  with unit reward on each leaf. Each leaf node corresponds to a terminating state and receives a unit reward. We consider this environment because the TV error can be computed exactly, making it suitable for validating our theory.

**Hypergrid** is a grid-based environment introduced by Bengio et al. (2021). It is parameterized by dimension  $D$ , side length  $H$ , and three reward coefficients  $R_0$ ,  $R_1$ , and  $R_2$ .

$$R(x) = R_0 + R_1 \prod_{i=1}^D \mathbb{I} \left( \left| \frac{x_i}{H-1} - 0.5 \right| > 0.25 \right) + R_2 \prod_{i=1}^D \mathbb{I} \left( \left| \frac{x_i}{H-1} - 0.5 \right| > 0.4 \right) \quad (22)$$

We use a  $R_0 = 10^{-2 \log_2(H/8)-1}$ ,  $R_1 = 0.5$ , and  $R_2 = 2.0$ .

**L14-RNA1**. The generated objects are RNA sequences of length 14. The reward function is a binding affinity to a human transcription factor, obtained via a pre-trained proxy model from Sinai et al. (2020). Following Kim et al.

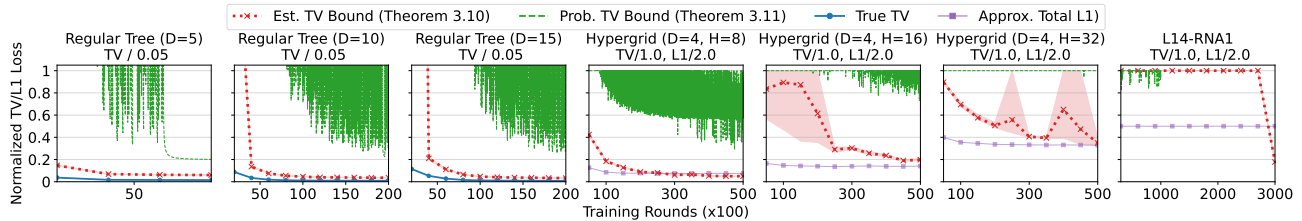


Figure 3. Derived TV bounds vs. empirical TV distances. We compare our theoretical bound with the measured distributional error. Shaded regions show the min-max range over 5 trials, each computed from a Monte Carlo estimate using 1,000 backward samples.

(2025b), we use a reward exponent of 20 and define modes as the top 0.01% quantile of  $R(x)$ . A diversity filtering with a Levenshtein distance threshold of 1 is enforced, resulting in 8,967 modes out of 268,435,456 possible end states.

### 5.1.2. BASELINES.

We compare against standard GFlowNet objectives: TB (Malkin et al., 2022a), DB (Bengio et al., 2023), FM (Bengio et al., 2021), and SubTB (Madan et al., 2023). For RQ2, we also include Adaptive Teacher (Teacher) (Kim et al., 2025b) and Weighted DB (WDB) (Silva et al., 2025). All methods utilize the same architectures and sampling budget. For L14-RNA1, we employ reward-prioritized replay (Shen et al., 2023) and  $\epsilon$ -greedy exploration (Malkin et al., 2022a). For the backward sampling, we use ground-truth terminating state distribution on Regular Tree and Hypergrid; on L14-RNA1, we utilize a buffer of the top-10,000 highest-reward states. The correspondence among environments, baselines, and RQs is summarized in Table 1.

### 5.2. Diagnosing Loss Instabilities (RQ1)

We introduce the *Max-to-Rest Loss Ratio* to quantify how strongly the highest-loss trajectory dominates a training batch. Figure 2 shows that batch losses can become heavily concentrated on a single trajectory, and that this concentration generally increases with task difficulty. In the medium-sized Hypergrid, we also observe pronounced spikes in the Max-to-Rest ratio that coincide with large fluctuations in the smoothed training loss. Together, these results confirm that loss spikes are pervasive during GFlowNet training and can destabilize optimization, motivating explicit stabilization mechanisms.

### 5.3. Stability and Mode Coverage Improvements (RQ2)

Table 2 shows that Stable GFlowNets matches the best baselines on easier Hypergrid and remains strongest on  $H = 32$  (trained for 30,000 rounds). On L14-RNA1 (trained for 50,000 rounds), our method achieves the highest *test-time* mode coverage, even though each update uses a half-batch of backward samples that are solely for certification and do not introduce new states; this indicates that stability alone

Table 2. Performance on Hypergrids and L14-RNA1. Metrics include Hypergrid  $L_1$  distance and L14-RNA1 mode counts (discovered in *Train* vs. *Test*). All test-time evaluations use  $10^5$  samples from the final policy  $P_F$ . (mean  $\pm$  std, 5 seeds)

Method	Hypergrid (Empirical Total $L_1 \downarrow$ )		L14-RNA1 (# Modes $\uparrow$ )	
	$D = 4, H = 16$	$D = 4, H = 32$	Train	Test
TB	$1.420 \pm 0.172$	$1.875 \pm 0.000$	$3206.4 \pm 554.9$	$591.8 \pm 41.2$
DB	$0.277 \pm 0.004$	$0.674 \pm 0.002$	$1989.6 \pm 55.3$	$498.8 \pm 43.4$
FM	$0.847 \pm 0.483$	$1.875 \pm 0.000$	$2807.0 \pm 442.1$	$554.2 \pm 49.5$
SubTB	<b><math>0.270 \pm 0.002</math></b>	$0.682 \pm 0.001$	$3357.0 \pm 135.6$	$619.8 \pm 16.5$
WDB	$1.883 \pm 0.000$	$1.926 \pm 0.001$	$2504.8 \pm 284.7$	$524.2 \pm 93.8$
Teacher	$0.295 \pm 0.002$	$0.747 \pm 0.018$	<b><math>5396.6 \pm 703.6</math></b>	$605.4 \pm 67.6$
<b>Stable (Ours)</b>	$0.276 \pm 0.002$	<b><math>0.663 \pm 0.001</math></b>	$3483.0 \pm 53.2$	<b><math>704.2 \pm 39.2</math></b>

can materially improve mode consolidation and coverage. Our method also shows the smallest variance across five seeds. In Appendix D, we further show that integrating our Stable GFlowNets with Adaptive Teacher further improves mode coverage.

### 5.4. Empirical Reflection of Our Theorems (RQ3)

We study the relationship between empirical distributional error and the probabilistic TV bound estimated from sampled trajectories. We train longer to track the Monte Carlo TV estimator (Theorem 3.10) and the probabilistic TV certificate (Theorem 3.11). Figure 3 shows that both provide useful monitoring signals. On Regular Tree, the Monte Carlo estimator tightly upper-bounds the true TV. On Hypergrid, both the certificate/estimation follow the  $L_1$ -based TV proxy and become more conservative at higher difficulty ( $H = 32$ ). On L14-RNA1, the  $L_1$  metric flattens even with 100,000 samples, while our bounds remain informative with only 1,000 samples and still reflect improvement. In practice, we recommend using the probabilistic certificate for training-time monitoring and the Monte Carlo estimator for data-efficient evaluation.

## 6. Conclusion and Discussion

This work clarifies what GFlowNet training losses do, and do not, reveal about global sampling fidelity. We show that loss spikes can occur even when the policy is near-optimal, then derive loss-to-TV guarantees and finite-sample TV

certificates from trajectory samples, turning loss monitoring into a probabilistic fidelity check. To stabilize training, we study reference flows as a principled way to control loss magnitudes and propose Stable GFlowNets, which adapt the reference flow while tracking a TV certificate.

Our guarantees currently rely on backward sampling, which could be difficult in continuous settings, and the probabilistic certificate can be overly conservative due to its worst-case dependence on the reference flow. Future work includes extending Theorem 3.6 to continuous state spaces and exploring hierarchical or latent representations as alternative stabilization mechanisms with comparable guarantees.

## Impact Statement

This paper presents work whose goal is to advance the field of Machine Learning. There are many potential societal consequences of our work, none which we feel must be specifically highlighted here.

## References

- Bengio, E., Jain, M., Korablyov, M., Precup, D., and Bengio, Y. Flow network based generative models for non-iterative diverse candidate generation. In *Advances in Neural Information Processing Systems*, 2021.
- Bengio, Y., Lahlou, S., Deleu, T., Hu, E. J., Tiwari, M., and Bengio, E. Gflownet foundations. *Journal of Machine Learning Research*, 2023.
- Chen, Y. and Mauch, L. Order-preserving GFlowNets. In *International Conference on Learning Representations*, 2024.
- He, H., Chang, C., Xu, H., and Pan, L. Looking backward: Retrospective backward synthesis for goal-conditioned GFlowNets. In *International Conference on Learning Representations*, 2025.
- Hu, R., Zhang, Y., Li, Z., and Huang, L. Beyond squared error: Exploring loss design for enhanced training of generative flow networks. In *International Conference on Learning Representations*, 2025.
- Ikram, Z., Pan, L., and Liu, D. Evolution guided generative flow networks. In *Transactions on Machine Learning Research*, 2025.
- Jain, M., Bengio, E., Hernandez-Garcia, A., Rector-Brooks, J., Dossou, B. F. P., Ekbote, C. A., Fu, J., Zhang, T., Kilgour, M., Zhang, D., Simine, L., Das, P., and Bengio, Y. Biological sequence design with GFlowNets. In *International Conference on Machine Learning*, 2022.
- Jang, H., Jang, Y., Kim, M., Park, J., and Ahn, S. Pessimistic backward policy for GFlowNets. In *Neural Information Processing Systems*, 2024.
- Kim, H., Kim, M., Choi, S., and Park, J. Genetic-guided gflownets for sample efficient molecular optimization. *Advances in Neural Information Processing Systems*, 2024a.
- Kim, M., Ko, J., Yun, T., Zhang, D., Pan, L., Kim, W., Park, J., Bengio, E., and Bengio, Y. Learning to scale logits for temperature-conditional GFlowNets. In *International Conference on Machine Learning*, 2024b.
- Kim, M., Yun, T., Bengio, E., Zhang, D., Bengio, Y., Ahn, S., and Park, J. Local search gflownets. In *International Conference on Learning Representations*, 2024c.
- Kim, M., Choi, S., Kim, H., Son, J., Park, J., and Bengio, Y. Ant colony sampling with GFlowNets for combinatorial optimization. In *International Conference on Artificial Intelligence and Statistics*, 2025a.
- Kim, M., Choi, S., Yun, T., Bengio, E., Feng, L., Rector-Brooks, J., Ahn, S., Park, J., Malkin, N., and Bengio, Y. Adaptive teachers for amortized samplers. In *International Conference on Learning Representations*, 2025b.
- Lahlou, S., Deleu, T., Lemos, P., Zhang, D., Volokhova, A., Hernández-García, A., Ezzine, L., Bengio, Y., and Malkin, N. A theory of continuous generative flow networks. In *International Conference on Machine Learning, Proceedings of Machine Learning Research*, 2023a.
- Lahlou, S., Viviano, J. D., Schmidt, V., and Bengio, Y. torchgfn: A Pytorch GFlowNet library. In *arXiv preprint arXiv:2305.14594*, 2023b.
- Lau, E., Vemgal, N., Precup, D., and Bengio, E. DGFN: Double generative flow networks. In *NeurIPS Workshop on Generative AI and Biology*, 2023.
- Lau, E., Lu, S., Pan, L., Precup, D., and Bengio, E. Qgfn: Controllable greediness with action values. In *Advances in neural information processing systems*, 2024.
- Lillicrap, T. P., Hunt, J. J., Pritzel, A., Heess, N., Erez, T., Tassa, Y., Silver, D., and Wierstra, D. Continuous control with deep reinforcement learning. In *arXiv preprint arXiv:1509.02971*, 2015.
- Madan, K., Rector-Brooks, J., Korablyov, M., Bengio, E., Jain, M., Nica, A. C., Bosc, T., Bengio, Y., and Malkin, N. Learning GFlowNets from partial episodes for improved convergence and stability. In *International Conference on Machine Learning*, 2023.
- Madan, K., Lamb, A., Bengio, E., Berseth, G., and Bengio, Y. Towards improving exploration through sibling

- augmented GFlowNets. In *International Conference on Learning Representations*, 2025.
- Malkin, N., Jain, M., Bengio, E., Sun, C., and Bengio, Y. Trajectory balance: Improved credit assignment in GFlowNets. In *Advances in Neural Information Processing Systems*, 2022a.
- Malkin, N., Lahlou, S., Deleu, T., Ji, X., Hu, E., Everett, K., Zhang, D., and Bengio, Y. Gflownets and variational inference. In *arXiv preprint arXiv:2210.00580*, 2022b.
- Nguyen, T. M., Tawfik, S. A., Tran, T., Gupta, S., Rana, S., and Venkatesh, S. Hierarchical gflownet for crystal structure generation. In *AI for Accelerated Materials Design-NeurIPS 2023 Workshop*, 2023.
- Pan, L., Malkin, N., Zhang, D., and Bengio, Y. Better training of GFlowNets with local credit and incomplete trajectories. In *International Conference on Machine Learning*, 2023a.
- Pan, L., Zhang, D., Courville, A., Huang, L., and Bengio, Y. Generative augmented flow networks. In *International Conference on Learning Representations*, 2023b.
- Pan, L., Jain, M., Madan, K., and Bengio, Y. Pre-training and fine-tuning generative flow networks. In *International Conference on Learning Representations*, 2024.
- Rombach, R., Blattmann, A., Lorenz, D., Esser, P., and Ommer, B. High-resolution image synthesis with latent diffusion models. In *IEEE/CVF conference on computer vision and pattern recognition*, 2022.
- Schulman, J., Levine, S., Abbeel, P., Jordan, M., and Moritz, P. Trust region policy optimization. In *International conference on machine learning*, 2015.
- Shalev-Shwartz, S. and Ben-David, S. *Understanding machine learning: From theory to algorithms*. Cambridge university press, 2014.
- Shen, M. W., Bengio, E., Hajiramezanali, E., Loukas, A., Cho, K., and Biancalani, T. Towards understanding and improving GFlowNet training. In *International Conference on Machine Learning*, 2023.
- Shen, T., Seo, S., Lee, G., Pandey, M., Smith, J. R., Cherkasov, A., Kim, W. Y., and Ester, M. Tacogfn: Target-conditioned gflownet for structure-based drug design. In *Transactions on Machine Learning Research*, 2024.
- Silva, T., de Souza da Silva, E., and Mesquita, D. On divergence measures for training gflownets. *Advances in Neural Information Processing Systems*, 2024.
- Silva, T., Alves, R. B., da Silva, E. d. S., Souza, A. H., Garg, V., Kaski, S., and Mesquita, D. When do gflownets learn the right distribution? In *International Conference on Learning Representations*, 2025.
- Sinai, S., Wang, R., Whatley, A., Slocum, S., Locane, E., and Kelsic, E. D. Adalead: A simple and robust adaptive greedy search algorithm for sequence design. 2020.
- Singh, S. P. and Yee, R. C. An upper bound on the loss from approximate optimal-value functions. *Machine Learning*, 1994.
- Song, Y., Durkan, C., Murray, I., and Ermon, S. Maximum likelihood training of score-based diffusion models. *Advances in neural information processing systems*, 2021.
- Sutton, R. S., Barto, A. G., et al. *Reinforcement learning: An introduction*. MIT press Cambridge, 1998.
- Tiapkin, D., Morozov, N., Naumov, A., and P Vetrov, D. Generative flow networks as entropy-regularized rl. In *International Conference on Artificial Intelligence and Statistics*, 2024.
- Zhang, D., Dai, H., Malkin, N., Courville, A. C., Bengio, Y., and Pan, L. Let the flows tell: Solving graph combinatorial problems with GFlowNets. In *Advances in Neural Information Processing Systems*, 2023.
- Zhang, D., Pan, L., Chen, R. T., Courville, A., and Bengio, Y. Distributional GFlowNets with quantile flows. In *Transactions on Machine Learning Research*, 2024.

## A. Proof of Propositions

**Proposition 3.3.** (*TV bound for incremental mode coverage over arbitrary state graph*). Let the reward added at each state in a subset  $\mathcal{X}_{sub}$  be  $R'(x)$ . We define the local true partition function  $Z_{\mathcal{Y} \subseteq \mathcal{X}}^* = \sum_{x \in \mathcal{Y}} R(x)$  and the local contrast ratio  $\Lambda_{\mathcal{Y}} = \frac{Z_{\mathcal{Y}}^*}{Z_{\mathcal{Y}}^* + \sum_{x \in \mathcal{Y}} R'(x)}$ . Then, we have

$$\frac{Z^* - Z_{\mathcal{X}_{sub}}^*}{Z^*} (1 - \Lambda_{\mathcal{X}}) \leq TV(P_T, \pi_{target}) \leq (1 - \Lambda_{\mathcal{X}})$$

*Proof.* To prove the upper bound, we use the standard definition of the Total Variation distance:

$$TV(P, Q) = \frac{1}{2} \sum_x |P(x) - Q(x)|$$

Substitute the expressions for the policies:

$$P_T(x) - \pi_{target}(x) = \frac{R(x)}{Z^*} - \frac{R'(x)}{Z^* + \sum_{x \in \mathcal{X}} R'(x)}$$

Substitute  $Z^* + \sum_{x \in \mathcal{X}} R'(x) = Z^* / \Lambda_{\mathcal{X}}$ :

$$P_T(x) - \pi_{target}(x) = \frac{(1 - \Lambda_{\mathcal{X}})R(x) - \Lambda_{\mathcal{X}}R'(x)}{Z^*}$$

Plug this back, we have

$$\begin{aligned} 2TV(P_T, \pi_{target}) &= \sum_{x \in \mathcal{X}} \left| \frac{(1 - \Lambda_{\mathcal{X}})R(x)}{Z^*} - \frac{\Lambda_{\mathcal{X}}R'(x)}{Z^*} \right| \\ &\leq \sum_{x \in \mathcal{X}} \frac{(1 - \Lambda_{\mathcal{X}})R(x)}{Z^*} + \sum_{x \in \mathcal{X}} \frac{\Lambda_{\mathcal{X}}R'(x)}{Z^*} \\ &= (1 - \Lambda_{\mathcal{X}}) + \frac{\sum_{x \in \mathcal{X}} R'(x)}{Z^* + \sum_{x \in \mathcal{X}} R'(x)} \\ &= 2(1 - \Lambda_{\mathcal{X}}) \end{aligned}$$

Divide both sides by 2, we get:

$$TV(P_T, \pi_{target}) \leq (1 - \Lambda_{\mathcal{X}})$$

To prove the lower bound, we use the alternative definition of TV distance:

$$TV(P, Q) = \sup_{X \subseteq \mathcal{X}} |P(X) - Q(X)|$$

This means the difference in probability mass on any specific subset  $X$  is a strict lower bound for the TV distance.

Let us choose the subset to be the unchanged region  $\mathcal{X}_{unc} = \mathcal{X} \setminus \mathcal{X}_{sub}$ . For any state  $x \in \mathcal{X}_{unc}$ ,  $R'(x) = 0$ .

We have

$$P_F(\mathcal{X}_{unc}) = \frac{\sum_{x \notin \mathcal{X}_{sub}} R(x)}{Z^*} = \frac{Z^* - Z_{\mathcal{X}_{sub}}^*}{Z^*}$$

$$\begin{aligned} \pi_{target}(\mathcal{X}_{unc}) &= \frac{Z^* - Z_{\mathcal{X}_{sub}}^*}{Z^* + \sum_{x \in \mathcal{X}} R'(x)} \\ &= \frac{\Lambda_{\mathcal{X}}(Z^* - Z_{\mathcal{X}_{sub}}^*)}{Z^*} \end{aligned}$$

$$\begin{aligned} TV(P_T, \pi_{target}) &\geq |P_T(\mathcal{X}_{unc}) - \pi_{target}(\mathcal{X}_{unc})| \\ &= \frac{(Z^* - Z_{\mathcal{X}_{sub}}^*)(1 - \Lambda_{\mathcal{X}})}{Z^*} \end{aligned}$$

□

**Proposition 3.4.** (*Loss scale via local contrast*). While the TV error depends on the aggregate  $\Lambda_{\mathcal{X}}$ , the supremum of the training loss is governed by the **worst-case** local contrast ratio, given by:

$$\sup |\mathcal{L}_{GFN}| = \left( \log \min_{\{x\} \subseteq \mathcal{X}_{sub}} \Lambda_{\{x\}} \right)^2$$

where  $GFN \in \{FM, DB, TB, subTB\}$ .

*Proof.* We assume the network parameters are currently at the optimum for the previous task. This means the current flow satisfies the balance equation for the old reward. Since only the rewards change and  $P_B$  is unchanged, substituting the pre-update state into the loss functions of the new task yields that all non-zero losses satisfy

$$\begin{aligned} \mathcal{L}_{FM}(x) &= \mathcal{L}_{DB}(s, x) = \mathcal{L}_{TB}(\tau \ni x) \\ &= \mathcal{L}_{subTB}(\tau_{t_1:t_2} \ni x) = \left( \log \frac{R(x)}{R(x) + R'(x)} \right)^2 \\ &= (\log \Lambda_{\{x\}})^2 \end{aligned}$$

□

The supremum of the loss over the entire state space is determined by the state  $x$  that maximizes this squared log term. Since  $\Lambda_{\{x\}} \leq 1$ , we have

$$\sup |\mathcal{L}_{GFN}| = \left( \log \min_{\{x\} \subseteq \mathcal{X}_{sub}} \Lambda_{\{x\}} \right)^2 \quad (23)$$

**Theorem 3.5.** (*Training loss to TV distance bound*). The relationship between the training loss bound and the resulting TV distance depends on the scope of the objective (trajectory-level vs. transition-level):

**Trajectory-level Objective.** If the trajectory loss is bounded by  $\mathcal{L}_{TB}(\tau) \leq c^2, \forall \tau \in \mathcal{T}$ , the TV error is bounded by:

$$TV(P_T, \pi_{target}) \leq 1 - \exp(-2c)$$

This bound is independent of the trajectory length, as TB optimizes the full path consistency directly.

**Transition-level Objective.** If the local transition loss is bounded by  $\mathcal{L}_{DB,FM}(s, s') \leq c^2$ , the global consistency relies on the accumulation of local estimates. For trajectories of maximum length  $L$ , the error bound degrades linearly with depth in the log-domain:

$$TV(P_T, \pi_{target}) \leq 1 - \exp(-2Lc)$$

*Proof.* We prove the bound for the TB loss, and note that the bounds for DM and FM can be converted into TB-loss bounds by multiplying the trajectory length  $L$ .

Let  $Z$  be the learnable partition function. When TB loss is bounded by  $c$ , then  $\forall \tau$  with  $x \in \tau$  and  $x \in \mathcal{X}$ , we have:

$$e^{-c} \leq \frac{Z P_F(\tau)}{R(x) P_B(\tau | x)} \leq e^c$$

Aggregate this inequality over all possible trajectories in the entire space  $\mathcal{T}$ , we have

$$\begin{aligned} e^{-c} &\leq \frac{Z}{Z^*} \leq e^c \\ Z^* e^{-c} &\leq Z \leq Z^* e^c \end{aligned}$$

Also from the TB definition, we have

$$\begin{aligned} P_F(\tau) &\geq e^{-c} \frac{R(x) P_B(\tau | x)}{Z} \\ &\geq e^{-c} \frac{R(x) P_B(\tau | x)}{e^c Z^*} \\ &\geq e^{-2c} \frac{R(x) P_B(\tau | x)}{Z^*} \end{aligned}$$

Sum overall trajectories that lead to  $x$ , we have

$$P_T(x) \geq e^{-2c} \frac{R(x)}{Z^*} = e^{-2c} \pi_{target}(x)$$

We use another alternative definition of TV distance:

$$TV(P, Q) = 1 - \sum_{x \in \mathcal{X}} \min(P, Q)$$

If  $P_T(x) \geq \pi_{target}(x)$ , then  $\min(P_T(x), \pi_{target}(x)) = \pi_{target}(x)$ . Since  $e^{-2c} \leq 1$ ,  $\pi_{target}(x) \geq e^{-2c} \pi_{target}(x)$ . If  $P_T(x) < \pi_{target}(x)$ , then  $\min(P_T(x), \pi_{target}(x)) = P_T(x) \geq e^{-2c} \pi_{target}(x)$ .

In both cases, we have

$$\min(P_T, \pi_{target}) \geq e^{-2c} \pi_{target}(x)$$

Substitute into the TV equation:

$$\begin{aligned} TV(P_T, \pi_{target}) &\leq 1 - \sum_{x \in \mathcal{X}} e^{-2c} \pi_{target}(x) \\ &= 1 - e^{-2c} \end{aligned}$$

□

**Theorem 3.6.** (Probabilistic TV bound via trajectory sampling). Given the ground-truth target distribution  $\pi_{target}$ , we define a target distribution over trajectories  $\hat{\pi}(\tau) = \pi_{target}(x_\tau) P_B(\tau | x_\tau)$ . Sample  $m$  trajectories  $\tau_1, \dots, \tau_m$  from  $\hat{\pi}$  independently by sampling  $x \sim \pi_{target}$  and  $\tau \sim P_B(\cdot | x)$ . Sample another  $n$  trajectories independently using  $P_F$ . Suppose we observe  $\mathcal{L}_{TB}(\tau_i) \leq c^2$  for all trajectories in both sets. With confidence  $1 - 2\alpha$ , the global TV error is bounded by:

$$TV(P_T, \pi_{target}) \leq \exp(2c) - 1 + \frac{\log(1/\alpha)}{m} + \frac{\log(1/\alpha)}{n}$$

*Proof.* Let  $P_F(\tau)$  be the forward policy's probability of trajectory  $\tau$ . Let  $\hat{\pi}(\tau)$  be the target trajectory distribution induced by the reward and backward policy:

$$\hat{\pi}(\tau) = \frac{R(x)}{Z^*} P_B(\tau | x) = \pi_{target}(x) P_B(\tau | x)$$

Note that the marginal of  $\hat{\pi}$  over states is exactly the target distribution:  $\sum_{\tau \rightarrow x} \hat{\pi}(\tau) = \pi_{target}(x)$ .

We define the ‘‘good’’ set of trajectories  $G_{\mathcal{T}} \subseteq \mathcal{T}$  as those satisfying the loss bound:

$$G_{\mathcal{T}} = \{\tau \in \mathcal{T} \mid \mathcal{L}_{TB}(\tau) \leq c^2\}$$

Let  $\epsilon = \hat{\pi}(G_{\mathcal{T}}^c)$  be the probability mass of bad trajectories under the target distribution. Since we observed  $m$  independent samples from  $\hat{\pi}$  and all fell into  $G_{\mathcal{T}}$ , the standard Probably Approximately Correct (PAC) bound via the Chernoff argument (Shalev-Shwartz & Ben-David, 2014) applies. With confidence  $1 - \alpha$ :

$$\epsilon \leq \frac{\log(1/\alpha)}{m}$$

Let  $\eta = P_F(G_{\mathcal{T}}^c)$  be the probability mass of bad trajectories under the forward policy. Similarly, since we observed  $n$  independent samples from  $P_F$  and all fell into  $G_{\mathcal{T}}$ , the standard PAC bound applies. With confidence  $1 - \alpha$ :

$$\eta \leq \frac{\log(1/\alpha)}{n}$$

By the union bound, we have  $\epsilon \leq \frac{\log(1/\alpha)}{m}$  and  $\eta \leq \frac{\log(1/\alpha)}{n}$  together hold with confidence  $1 - 2\alpha$ .

For any good trajectory  $\tau \in G_{\mathcal{T}}$ , the condition  $\mathcal{L}_{TB}(\tau) \leq c^2$  implies:

$$\left| \log \frac{Z P_F(\tau)}{R(x) P_B(\tau|x)} \right| \leq c$$

$$e^{-c} \leq \frac{K P_F(\tau)}{\hat{\pi}(\tau)} \leq e^c$$

where  $K = \frac{Z}{Z^*}$ .

Now we derive the bound for  $K$ , note

$$K \sum_{\tau \in G_{\mathcal{T}}} P_F(\tau) \geq \sum_{\tau \in G_{\mathcal{T}}} e^{-c} \hat{\pi}(\tau) = e^{-c} (1 - \epsilon)$$

Since  $\sum_{\tau \in G_{\mathcal{T}}} P_F(\tau) \leq 1$ , we have

$$K \geq e^{-c} (1 - \epsilon)$$

So  $\frac{P_F(\tau)}{\hat{\pi}(\tau)}$  satisfies

$$\frac{P_F(\tau)}{\hat{\pi}(\tau)} \leq \frac{1}{1 - \epsilon} e^{2c}$$

The TV distance between the two distributions over trajectories is bounded by:

$$2TV(P_F, \hat{\pi}) = \sum_{\tau \in G_{\mathcal{T}}} |P_F(\tau) - \hat{\pi}(\tau)| + \sum_{\tau \in G_{\mathcal{T}}^c} |P_F(\tau) - \hat{\pi}(\tau)|$$

For the first term  $\sum_{\tau \in G_{\mathcal{T}}} |P_F(\tau) - \hat{\pi}(\tau)|$ , we split the good set  $G_{\mathcal{T}}$  into  $G_{\mathcal{T}}^+$  and  $G_{\mathcal{T}}^-$  such that

$$P_F(\tau) \geq \hat{\pi}(\tau), \forall \tau \in G_{\mathcal{T}}^+$$

$$P_F(\tau) < \hat{\pi}(\tau), \forall \tau \in G_{\mathcal{T}}^-$$

We have

$$\begin{aligned} & \sum_{\tau \in G_{\mathcal{T}}} |P_F(\tau) - \hat{\pi}(\tau)| \\ &= \sum_{\tau \in G_{\mathcal{T}}^+} (P_F(\tau) - \hat{\pi}(\tau)) + \sum_{\tau \in G_{\mathcal{T}}^-} (\hat{\pi}(\tau) - P_F(\tau)) \\ &= \sum_{\tau \in G_{\mathcal{T}}^+} (P_F(\tau) - \hat{\pi}(\tau)) + (1 - \epsilon) - \sum_{\tau \in G_{\mathcal{T}}^+} \hat{\pi}(\tau) \\ & \quad - (1 - \eta) + \sum_{\tau \in G_{\mathcal{T}}^+} P_F(\tau) \\ &= 2 \sum_{\tau \in G_{\mathcal{T}}^+} (P_F(\tau) - \hat{\pi}(\tau)) + \eta - \epsilon \\ &= 2 \sum_{\tau \in G_{\mathcal{T}}^+} \hat{\pi}(\tau) \left( \frac{P_F(\tau)}{\hat{\pi}(\tau)} - 1 \right) + \eta - \epsilon \\ &\leq 2(1 - \epsilon) \left( \frac{1}{1 - \epsilon} e^{2c} - 1 \right) + \eta - \epsilon \\ &= 2(e^{2c} - 1) + \eta + \epsilon \end{aligned}$$

For the second term  $\sum_{\tau \in G_{\mathcal{T}}^c} |P_F(\tau) - \hat{\pi}(\tau)|$ , we directly use the triangle inequality and get

$$\begin{aligned} \sum_{\tau \in G_{\mathcal{T}}^c} |P_F(\tau) - \hat{\pi}(\tau)| &\leq \sum_{\tau \in G_{\mathcal{T}}^c} P_F(\tau) + \sum_{\tau \in G_{\mathcal{T}}^c} \hat{\pi}(\tau) \\ &= \eta + \epsilon \end{aligned}$$

Combine the first term and the second term, we have

$$TV(P_F, \hat{\pi}) \leq (e^{2c} - 1) + \epsilon + \eta$$

For the TV distance between marginal distributions, we have

$$TV(P_T, \pi_{target}) = \frac{1}{2} \sum_x |P_T(x) - \pi_{target}(x)|$$

Since  $P_T(x) = \sum_{\tau \rightarrow x} P_F(\tau)$  and  $\pi_{target}(x) = \sum_{\tau \rightarrow x} \hat{\pi}(\tau)$ :

$$\begin{aligned} |P_T(x) - \pi_{target}(x)| &= \left| \sum_{\tau \rightarrow x} (P_F(\tau) - \hat{\pi}(\tau)) \right| \\ &\leq \sum_{\tau \rightarrow x} |P_F(\tau) - \hat{\pi}(\tau)| \end{aligned}$$

Summing over all  $x$ :

$$\begin{aligned}
 TV(P_T, \pi_{target}) &\leq \frac{1}{2} \sum_x \sum_{\tau \rightarrow x} |P_F(\tau) - \hat{\pi}(\tau)| \\
 &= TV(P_F, \hat{\pi}) \\
 &\leq (e^{2c} - 1) + \epsilon + \eta \\
 &\leq (e^{2c} - 1) + \\
 &\quad \frac{\log(1/\alpha)}{m} + \frac{\log(1/\alpha)}{n}
 \end{aligned}$$

□

**Corollary 3.7.** (Subgraph Certification via trajectory sampling). Let  $\mathcal{X}_{sub} \subseteq \mathcal{X}$  be a subset of end-states. Define the restricted target distribution over  $\mathcal{X}_{sub}$  by  $\pi_{target}^{sub}(x) = \frac{\sum_{x \in \mathcal{X}_{sub}} R(x)}{\sum_{x \in \mathcal{X}} R(x)}$ , the corresponding restricted target trajectory distribution as  $\hat{\pi}_{sub}(\tau) = \pi_{target}^{sub}(x_\tau) P_B(\tau | x_\tau)$ . Sample  $m$  trajectories  $\tau_1, \dots, \tau_m$  from  $\hat{\pi}_{sub}$ . Sample another  $n$  trajectories that end within  $\mathcal{X}_{sub}$  independently using  $P_F$ . Suppose we observe  $\mathcal{L}_{TB}(\tau_i) \leq c^2$  for all trajectories in both sets. Let  $P_T^{sub}$  denote the terminal flow  $P_T$  renormalized to  $\mathcal{X}_{sub}$ . Then, with confidence  $1 - 2\alpha$ ,

$$TV(P_T^{sub}, \pi_{target}^{sub}) \leq \exp(2c) - 1 + \frac{\log(1/\alpha)}{m} + \frac{\log(1/\alpha)}{n}$$

*Proof.* To prove this corollary, we first develop a mapping from the global forward policy  $P_F$  and partition function  $Z$  to the subgraph restricted counterparts  $P_F^{sub}$  and  $Z_{sub}$ .

Consider the subgraph induced by  $\mathcal{X}_{sub}$ . We have the partition function for the subgraph

$$Z_{sub} = \sum_{x \in \mathcal{X}_{sub}} F_{state}(x) = Z \sum_{x \in \mathcal{X}_{sub}} P_T(x)$$

The backward policy over the subgraph yields the same value as the global one, i.e.,  $P_B^{sub} = P_B$ . The forward policy over this subgraph  $P_F^{sub}$  can be represented as the forward policy conditioned on the trajectory ending in the subgraph:

$$P_F^{sub}(\tau) = P_F(\tau | x_\tau \in \mathcal{X}_{sub}) = \frac{P_F(\tau)}{\sum_{x \in \mathcal{X}_{sub}} P_T(x)}$$

Now we map the TB loss to the subgraph context, we have the TB loss over the subgraph become:

$$\begin{aligned}
 \mathcal{L}_{TB}^{sub}(\tau) &= \left( \log \frac{Z_{sub} P_F^{sub}(\tau)}{R(x) P_B^{sub}(\tau|x)} \right)^2 \\
 &= \left( \log \frac{Z P_F(\tau) \sum_{x \in \mathcal{X}_{sub}} P_T(x)}{R(x) P_B(\tau|x) \sum_{x \in \mathcal{X}_{sub}} P_T(x)} \right)^2 \\
 &= \left( \log \frac{Z P_F(\tau)}{R(x) P_B(\tau|x)} \right)^2 \leq c^2
 \end{aligned}$$

Since all preconditions of Theorem 3.6 are satisfied for the subgraph, we apply it directly to obtain the desired bound. □

**Theorem 3.10.** (Fidelity trade-off under reference flow). The fidelity of the recovered policy depends on the ratio between the training loss and the augmentation magnitude. Let the total reference flow be  $\Delta = \sum_{\tau \in \mathcal{T}} \delta(\tau)$ . If the reference training loss is bounded by  $\mathcal{L}_{aug}(\tau) \leq c^2$ , the TV error of the learned flow  $P_F$  is bounded by:

$$TV(P_T, \pi_{target}) \leq (1 - \exp(-2c))(1 + \frac{\Delta}{Z^*})$$

*Proof.* Define  $\delta(x) = \sum_{\tau \ni x} \delta(\tau)$ , note  $\Delta = \sum_{x \in \mathcal{X}} \delta(x)$ . We have the target distribution under reference flows as:

$$\pi_{aug}(x) = \frac{R(x) + \delta(x)}{Z^* + \Delta}$$

From the proof of Theorem 3.5, we have

$$\frac{F_{state}(x) + \delta(x)}{Z^* + \Delta} \geq \frac{e^{-2c}(R(x) + \delta(x))}{Z^* + \Delta}$$

$$F_{state}(x) + \delta(x) \geq e^{-2c}(R(x) + \delta(x))$$

$$\begin{aligned}
 F_{state}(x) &\geq e^{-2c}R(x) + (e^{-2c} - 1)\delta(x) \\
 &= R(x) \left( e^{-2c} - 1 + 1 + (e^{-2c} - 1) \frac{\delta(x)}{R(x)} \right) \\
 &= R(x) \left( 1 + (e^{-2c} - 1) \left( 1 + \frac{\delta(x)}{R(x)} \right) \right)
 \end{aligned}$$

Divide both sides by  $Z^*$ , we have

$$P_T(x) \geq \left( 1 + (e^{-2c} - 1) \left( 1 + \frac{\delta(x)}{R(x)} \right) \right) \pi_{target}(x)$$

Since  $\left( 1 + (e^{-2c} - 1) \left( 1 + \frac{\delta(x)}{R(x)} \right) \right) < 1$  we have

$$\min(P_T, \pi_{target}) \geq \left( 1 + (e^{-2c} - 1) \left( 1 + \frac{\delta(x)}{R} \right) \right) \pi_{target}$$

We sum the lower bound over all  $x$  and get

$$\begin{aligned}
 \sum_{x \in \mathcal{X}} \min(P_T(x), \pi(x)) &\geq \underbrace{\sum_{x \in \mathcal{X}} \pi_{target}(x)}_1 - \\
 &\quad (1 - e^{-2c}) \underbrace{\sum_{x \in \mathcal{X}} \pi_{target}(x) \left( 1 + \frac{\delta(x)}{R(x)} \right)}_{\text{The Critical Term}}
 \end{aligned}$$

Now we simplify the critical term by substituting  $\pi_{target}(x) = \frac{R(x)}{Z^*}$ :  $n$

$$\begin{aligned} \sum_{x \in \mathcal{X}} \pi_{target}(x) \left(1 + \frac{\delta(x)}{R(x)}\right) &= \sum_{x \in \mathcal{X}} \frac{R(x) + \delta(x)}{Z^*} \\ &= 1 + \frac{\Delta}{Z^*} \end{aligned}$$

Substitute into the TV definition

$$TV(P_T, \pi_{target}) \leq (1 - e^{-2c}) \left(1 + \frac{\Delta}{Z^*}\right)$$

□

**Theorem 3.11.** (Probabilistic TV bound of reference flow). *Sample  $m$  trajectories  $\tau_1, \dots, \tau_m$  independently from the target  $\hat{\pi}$ , sample another  $n$  trajectories  $\tau_{m+1}, \dots, \tau_{m+n}$  independently using  $P_F$ , we compute the reference flow  $\delta(\tau_i)$  required to bound the reference loss by  $c^2$  according to Equation (17). When  $M := \max_{i \in \{1, \dots, m+n\}} \frac{\delta(\tau_i)}{\mathcal{R}(\tau_i)} < \frac{1}{\exp(c)-1}$ , with confidence  $1 - 2\alpha$ , the global TV error is bounded by:*

$$\begin{aligned} TV(P_T, \pi_{target}) &\leq \frac{\log(1/\alpha)}{m} + \frac{\log(1/\alpha)}{n} \\ &+ \left( \frac{\exp(c) + (\exp(c) - 1)M}{\exp(-c) - (1 - \exp(-c))M} - 1 \right) \end{aligned}$$

*Proof.* We observe that the global ratio  $\frac{\Delta}{Z^*}$  can be expressed as an expectation over the target distribution  $\hat{\pi}(\tau) = \frac{\mathcal{R}(\tau)}{Z^*}$ . By multiplying and dividing by  $\mathcal{R}(\tau)$  inside the summation:

$$\begin{aligned} \frac{\Delta}{Z^*} &= \sum_{\tau \in \mathcal{T}} \frac{\delta(\tau)}{Z^*} \\ &= \sum_{\tau \in \mathcal{T}} \frac{\mathcal{R}(\tau)}{Z^*} \cdot \frac{\delta(\tau)}{\mathcal{R}(\tau)} \\ &= \mathbb{E}_{\tau \sim \hat{\pi}} \left[ \frac{\delta(\tau)}{\mathcal{R}(\tau)} \right] \end{aligned}$$

This identifies the total reference mass relative to  $Z^*$  as the expected “relative correction” required under the target distribution.

We define the “good” set of trajectories  $G_{\mathcal{T}} \subseteq \mathcal{T}$  as those satisfying the loss bound:

$$G_{\mathcal{T}} = \{r \in \mathcal{T} \mid \delta(\tau) \leq M := \max_{i \in \{1, 2, \dots, m+n\}} \frac{\delta(\tau_i)}{\mathcal{R}(\tau_i)}\}$$

Let  $\epsilon = \hat{\pi}(G_{\mathcal{T}}^c)$  be the probability mass of bad trajectories under the target distribution.  $\eta = P_F(G_{\mathcal{T}}^c)$  be the probability mass of bad trajectories under the forward policy. Using PAC and union bound, we have with confidence  $1 - 2\alpha$ ,

$$\epsilon \leq \frac{\log(1/\alpha)}{m}, \quad \eta \leq \frac{\log(1/\alpha)}{n}$$

For any good trajectory  $\tau \in G_{\mathcal{T}}$ , we have

$$\left| \log \frac{Z P_F(\tau) + \delta(\tau)}{R(x) P_B(\tau|x) + \delta(\tau)} \right| \leq c$$

$$e^{-c} \leq \frac{K P_F(\tau) + \delta(\tau)/Z^*}{\hat{\pi}(\tau) + \delta(\tau)/Z^*} \leq e^c$$

where  $K = \frac{Z}{Z^*}$

Now we derive the bound for  $K$ , since  $\sum_{\tau \in G_{\mathcal{T}}} P_F(\tau) \leq 1$ ,

$$\begin{aligned} K &\geq \sum_{\tau \in G_{\mathcal{T}}} e^{-c} \hat{\pi}(\tau) - (1 - e^{-c}) \sum_{\tau \in G_{\mathcal{T}}} \frac{\delta(\tau)}{Z^*} \\ &= e^{-c}(1 - \epsilon) - (1 - e^{-c}) \sum_{\tau \in G_{\mathcal{T}}} \frac{\mathcal{R}(\tau)}{Z^*} \frac{\delta(\tau)}{\mathcal{R}(\tau)} \\ &\geq e^{-c}(1 - \epsilon) - (1 - e^{-c})M \sum_{\tau \in G_{\mathcal{T}}} \frac{\mathcal{R}(\tau)}{Z^*} \\ &\geq e^{-c}(1 - \epsilon) - (1 - e^{-c})(1 - \epsilon)M \end{aligned}$$

Since  $M < \frac{1}{e^c - 1}$ , we have

$$(1 - \epsilon) (e^{-c} - (1 - e^{-c})M) > 0$$

Plug this back, we get

$$P_F(\tau) \leq \frac{e^c \hat{\pi}(\tau) + (e^c - 1)\delta(\tau)/Z^*}{(1 - \epsilon)(e^{-c} - (1 - e^{-c})M)}$$

$$\begin{aligned} \frac{P_F(\tau)}{\hat{\pi}(\tau)} &\leq \frac{e^c + (e^c - 1)\delta(\tau)/\mathcal{R}(\tau)}{(1 - \epsilon)(e^{-c} - (1 - e^{-c})M)} \\ &\leq \frac{e^c + (e^c - 1)M}{(1 - \epsilon)(e^{-c} - (1 - e^{-c})M)} \end{aligned}$$

The TV distance between the two distributions over trajectories is bounded by:

$$\begin{aligned} 2TV(P_F, \hat{\pi}) &= \sum_{\tau \in G_{\mathcal{T}}} |P_F(\tau) - \hat{\pi}(\tau)| + \\ &\quad \sum_{\tau \in G_{\mathcal{T}}^c} |P_F(\tau) - \hat{\pi}(\tau)| \end{aligned}$$

For the first term  $\sum_{\tau \in G_{\mathcal{T}}} |P_F(\tau) - \hat{\pi}(\tau)|$ , we split the good set  $G_{\mathcal{T}}$  into  $G_{\mathcal{T}}^+$  and  $G_{\mathcal{T}}^-$  such that

$$P_F(\tau) \geq \hat{\pi}(\tau), \forall \tau \in G_{\mathcal{T}}^+$$

$$P_F(\tau) < \hat{\pi}(\tau), \forall \tau \in G_{\mathcal{T}}^-$$

We have

$$\begin{aligned} & \sum_{\tau \in G_{\mathcal{T}}} |P_F(\tau) - \hat{\pi}(\tau)| \\ &= \sum_{\tau \in G_{\mathcal{T}}^+} (P_F(\tau) - \hat{\pi}(\tau)) + \sum_{\tau \in G_{\mathcal{T}}^-} (\hat{\pi}(\tau) - P_F(\tau)) \\ &= \sum_{\tau \in G_{\mathcal{T}}^+} (P_F(\tau) - \hat{\pi}(\tau)) + (1 - \epsilon) - \sum_{\tau \in G_{\mathcal{T}}^+} \hat{\pi}(\tau) \\ & \quad - (1 - \eta) + \sum_{\tau \in G_{\mathcal{T}}^+} P_F(\tau) \\ &= 2 \sum_{\tau \in G_{\mathcal{T}}^+} (P_F(\tau) - \hat{\pi}(\tau)) + \eta - \epsilon \\ &= 2 \sum_{\tau \in G_{\mathcal{T}}^+} \hat{\pi}(\tau) \left( \frac{P_F(\tau)}{\hat{\pi}(\tau)} - 1 \right) + \eta - \epsilon \\ &\leq 2(1 - \epsilon) \left( \frac{e^c + (e^c - 1)M}{(1 - \epsilon)(e^{-c} - (1 - e^{-c})M)} - 1 \right) + \eta - \epsilon \\ &= 2 \left( \frac{e^c + (e^c - 1)M}{e^{-c} - (1 - e^{-c})M} - 1 \right) + \eta + \epsilon \end{aligned}$$

For the second term  $\sum_{\tau \in G_{\mathcal{T}}^c} |P_F(\tau) - \hat{\pi}(\tau)|$ , we directly use the triangle inequality and get

$$\begin{aligned} \sum_{\tau \in G_{\mathcal{T}}^c} |P_F(\tau) - \hat{\pi}(\tau)| &\leq \sum_{\tau \in G_{\mathcal{T}}^c} P_F(\tau) + \sum_{\tau \in G_{\mathcal{T}}^c} \hat{\pi}(\tau) \\ &= \eta + \epsilon \end{aligned}$$

Combine the first term and the second term, we have

$$TV(P_F, \hat{\pi}) \leq \left( \frac{e^c + (e^c - 1)M}{e^{-c} - (1 - e^{-c})M} - 1 \right) + \epsilon + \eta$$

For the TV distance between marginal distributions, we have

$$TV(P_T, \pi_{target}) = \frac{1}{2} \sum_x |P_T(x) - \pi_{target}(x)|$$

Since  $P_T(x) = \sum_{\tau \rightarrow x} P_F(\tau)$  and  $\pi_{target}(x) =$

$$\sum_{\tau \rightarrow x} \hat{\pi}(\tau):$$

$$\begin{aligned} |P_T(x) - \pi_{target}(x)| &= \left| \sum_{\tau \rightarrow x} (P_F(\tau) - \hat{\pi}(\tau)) \right| \\ &\leq \sum_{\tau \rightarrow x} |P_F(\tau) - \hat{\pi}(\tau)| \end{aligned}$$

Summing over all  $x$ :

$$\begin{aligned} TV(P_T, \pi_{target}) &\leq \frac{1}{2} \sum_x \sum_{\tau \rightarrow x} |P_F(\tau) - \hat{\pi}(\tau)| \\ &= TV(P_F, \hat{\pi}) \\ &\leq \left( \frac{e^c + (e^c - 1)M}{e^{-c} - (1 - e^{-c})M} - 1 \right) + \epsilon + \eta \\ &\leq \left( \frac{e^c + (e^c - 1)M}{e^{-c} - (1 - e^{-c})M} - 1 \right) + \\ & \quad \frac{\log(1/\alpha)}{m} + \frac{\log(1/\alpha)}{n} \end{aligned}$$

□

## B. Connection Between Our Theoretical Findings and Existing GFlowNets Training Approaches

We analyze existing advances in GFlowNet training through the lens of our theoretical results, interpreting how diverse algorithmic design choices implicitly improve stability and certification performance.

- **Annealing Schedules.** Kim et al. (2024b) proposed scaling logits (temperature annealing), while Chen & Mauch (2024) used order-preserving flows. While these methods do not explicitly use a reference flow variable  $\delta$ , they achieve a similar stabilizing effect by manipulating the target distribution. High initial temperatures flatten the energy landscape, keeping log-ratios  $\log \frac{P_F}{\mathcal{R}}$  small, thereby mitigating abrupt increases in flow mismatch and postponing large loss explosions.
- **Sub-trajectory and Partial Losses.** Madan et al. (2023) introduced Sub-Trajectory Balance (SubTB) to assign credit to partial trajectories, while Shen et al. (2023) parametrized policies over transitions. By decomposing the global trajectory loss into local constraints, these methods reduce the variance of the flow mismatch. In our framework, lower variance implies that a smaller reference flow  $\delta(\tau)$  is sufficient to satisfy the stability condition  $\mathcal{L} \leq c^2$ , directly improving the certification performance.

- **Divergence and Distributional Objectives.** Distributional objectives (Zhang et al., 2024) and alternative divergence-based losses (Silva et al., 2024; Hu et al., 2025) replace mean squared flow mismatches with smoother optimization criteria. These formulations suppress extreme gradient spikes, implicitly bounding the loss and improving training stability.
- **Guided Exploration.** GAFN (Pan et al., 2023b) and Double GFN (Lau et al., 2023) inject stochasticity through reference transitions or dual-network designs. By forcing the policies to stay random enough to keep looking for better solutions, they promote the representativeness of end-state coverage and therefore improve verification effectiveness. Kim et al. (2024c) utilized backward sampling for local search around discovered modes. Lau et al. (2024) combined GFlowNets with Q-functions, while Ikram et al. (2025), Kim et al. (2024a), and Kim et al. (2025a) integrated evolutionary and genetic algorithms to guide exploration. Additionally, Kim et al. (2025b) leveraged a teacher policy to focus sampling specifically on regions where the student policy exhibits high loss. These methods aggressively expand the support of the discovered subgraph  $\mathcal{X}_{sub}$ . In the context of our bounds, they implicitly sample more high-loss/undervisited “backward” sampled trajectories associated with high reward. By encouraging the training process to observe and minimize loss on these specific trajectories, these methods improve the verification bound.
- **Backward Policy Optimization.** Jang et al. (2024) proposed pessimistic backward policies. Through the lens of Theorem 3.6, this biases  $P_B$  to align backward samples with forward-visited trajectories. This alignment improves verification performance.
- **Replay Buffer.** Madan et al. (2025) introduced reward-prioritized replay, which, through the lens of Theorem 3.6, biases the empirical sampling distribution toward backward-sampled trajectories (that terminate in high-reward states) and repeatedly revisiting these trajectories helps improve the verification bounds.
- **Structure and Pre-training.** Nguyen et al. (2023) and Shen et al. (2024) formulated GFlowNets for hierarchical and conditional generation, while Pan et al. (2024) utilized pre-training pipelines. He et al. (2025) further extended this to retrospective synthesis. These methods mitigate the “incremental mode coverage” challenge described in Section 3.1. By decomposing the search space or conditioning on specific goals, these methods increase the local contrast ratio  $\Lambda_{\mathcal{X}}$  in Proposition 3.4). Theoretically, this ensures high-reward states maintain non-negligible probability, preventing loss explosions.

## C. Experimental Details

### C.1. Implementations

We implement GFlowNet training with DB, FM, TB, and SubTB losses following Lahlou et al. (2023b). For adaptive teacher networks, we adopt the implementation of Kim et al. (2025b). For weighted detailed balance (WDB), we follow Silva et al. (2025) by reweighting each transition’s loss inversely by the number of terminating states reachable from that transition, and then normalizing the weights within the sampled trajectory so they sum to 1. We parameterize  $P_F$ ,  $P_B$ , and the flow function  $F$  with the same MLP architecture but separate parameters.

For optimization stability, we follow Shen et al. (2023) and clip gradient norms to 10.0 and clamp policy logits to  $[-50, 50]$ . Although gradient clipping is not enabled in the original torchgfn<sup>1</sup> code, we found it consistently improves baseline stability and performance; we therefore apply it to all methods to ensure a fair comparison and to isolate the gains from Stable GFlowNets. With gradient clipping, we also find that model performance is less sensitive to partition-function initialization, so we fix initial  $\log Z_\theta = 0$  and do not tune it across environments.

For the L14-RNA1 task, we use a reward-prioritized replay buffer of size 1,000 following Kim et al. (2025b). We also adopt  $\epsilon$ -greedy exploration (Malkin et al., 2022b) with  $\epsilon = 0.05$ : with probability 0.05, the forward policy takes a uniformly random action instead of sampling from  $P_{F_\theta}$ .

All RQ2 experiments are repeated over five random seeds 470, 3825, 4444, 8888, 9528. For RQ1, we use the results obtained by seed 470. For RQ3, we run the extended Hypergrid and L14-RNA1 experiments with seed 0 due to the limit of our computational resources.

### C.2. Hyperparameters

For Regular Tree and Hypergrid, we use an MLP with two hidden layers of 256 units each; the Hypergrid architecture matches the setting in Malkin et al. (2022a). For L14-RNA1, we follow Kim et al. (2025b) and use a hidden size of 128 for short runs (50,000 training rounds). Prior work typically evaluates over fewer rounds, but in our longer runs we find wider networks perform better; therefore for extended training (300,000 rounds), we use a hidden size of 256.

We use a batch size of 32. The learning rate for  $\log Z_\theta$  is set to be  $100\times$  the learning rate of the forward and backward policies. Hyperparameters are selected by grid search: policy learning rates in  $\{10^{-4}, 5 \times 10^{-4}, 10^{-3}\}$  and activation functions in ReLU, LeakyReLU. We use a learning

<sup>1</sup>[https://github.com/GFNorg/torchgfn/blob/master/tutorials/examples/train\\_hypergrid.py](https://github.com/GFNorg/torchgfn/blob/master/tutorials/examples/train_hypergrid.py)

rate of  $10^{-3}$  for Regular Tree and  $10^{-4}$  for Hypergrid and L14-RNA1, with LeakyReLU in all experiments.

For Stable GFlowNets, we split each batch evenly: half (i.e., 16 trajectories) is from forward sampling and half from backward sampling. We set the TV target to  $d = 0.01$  and the confidence level to 0.95, which is relatively strict. For L14-RNA1, we set the patience parameter to 10 and the high-reward state size to  $|\mathcal{X}_{\text{sub}}| = 10,000$ . Under these settings, only the simplest Regular Tree environment terminates early when the certification condition is met.

## D. Additional Experimental Results

### D.1. Learned patterns in the Hypergrid environment in Figure 2

Figures 4-6 visualize samples from the trained models at different training stages. These snapshots help explain the larger fluctuations and higher max-to-rest loss ratios observed in the  $H=16$  Hypergrid. In particular, the  $H=16$  setting discovers multiple modes over time, whereas in  $H=32$  both TB and FM typically concentrate on a single mode. This yields smoother training dynamics in  $H=32$ , albeit with mode collapse. Overall, these results indicate that instability is driven not only by reward sparsity but also by the difficulty of discovering additional high-reward goals: once an existing mode is well fit, the max-to-rest ratio can spike when a new mode is first uncovered.

We also find that DB performs better in this setting. Although it uses the same transitions as TB, DB has more parameters to learn (since it uses the state flow estimator rather than the partition function), which slows policy convergence; in hard-to-explore environments like Hypergrid, this implicit slowdown can be beneficial. However, RQ2 (Table 2) shows DB is not uniformly superior. In L14-RNA1, DB learns too slowly under  $\epsilon$ -exploration, resulting in poorer mode discovery. In contrast, from Table 2, WDB accelerates learning via reweighting, and this faster optimization is associated with improved exploration in L14-RNA1, yielding more discovered modes over training.

### D.2. Aggregation for updating the loss threshold in Stable GFlowNets

We compare different aggregation rules for the batch loss used in the loss-threshold update (Equation (20)) under the RQ2 setting, including the maximum, mean, and median. Overall, the mean and maximum perform similarly well, with the maximum performing slightly better.

### D.3. Integrate Adaptive Teacher and Stable GFlowNets

We evaluate a simple integration of Stable GFlowNets with the Adaptive Teacher method of Kim et al. (2025b). In

Table 3. Effect of loss-threshold aggregation on Hypergrids and L14-RNA1. We report Hypergrid  $L_1$  distance and L14-RNA1 mode counts (discovered in *Train* vs. *Test*). All test-time evaluations use  $10^5$  samples from the final forward policy  $P_F$  (mean  $\pm$  std over 5 seeds). For L14-RNA1, we use a larger MLP with hidden-layer widths 256/256, whereas Table 2 uses 128/128.

Aggregation	Hypergrid (Empirical Total $L_1$ $\downarrow$ )		L14-RNA1 (# Modes $\uparrow$ )	
	$D = 4, H = 16$	$D = 4, H = 32$	Train	Test
Max	$0.277 \pm 0.004$	$0.663 \pm 0.003$	$3494.8 \pm 197.6$	$730.6 \pm 38.7$
Mean	$0.276 \pm 0.003$	$0.672 \pm 0.005$	$3454.2 \pm 102.1$	$714.6 \pm 45.9$
Median	$1.885 \pm 0.000$	$1.875 \pm 0.000$	$3359.4 \pm 212.7$	$646.4 \pm 63.0$

addition to forward- and backward-sampled trajectories, we include a third set of teacher-sampled trajectories. Each batch contains 16 forward, 16 backward, and 16 teacher trajectories (batch size 48). We use the same batch size for all baselines to ensure a fair comparison.

Figure 7 reports the long-run results on L14-RNA1. StableTeacher discovers 8,858 modes during training, covering 98.78% of the modes in this environment while using a sample budget of only 5.36% of the end state space. Measured by the total reward mass accumulated by the Top-10K terminal states, StableTeacher also achieves higher values than Teacher early in training. The smoothed loss curves indicate that StableTeacher responds systematically when new modes are uncovered, while maintaining a more balanced max-to-rest ratio throughout training. In contrast, Teacher shows an increasing max-to-rest ratio later in training, suggesting that a small number of trajectories dominate the batch as high-reward modes emerge, which is consistent with less stable optimization.

We also compare TB against Stable GFlowNets in long runs. With gradient clipping, TB performs well early on but tends to saturate, becoming less likely to discover additional modes. Its training loss continues to decrease, yet exploration slows. Stable GFlowNets, in contrast, continue to adapt as new modes appear: their loss remains higher than TB in later stages, reflecting active correction driven by newly discovered high-reward outcomes, whereas standard TB tends to settle into its “comfort zone”. We observe a concurrent increase in the max-to-rest ratio, which we hypothesize is transient as the loss threshold increases and will subside once the newly discovered modes are sufficiently represented in the training distribution.

Collectively, these results suggest that Stable GFlowNets enables stronger incremental mode coverage, complementing aggressive exploration in settings where sampling from the full set of terminating states is difficult.

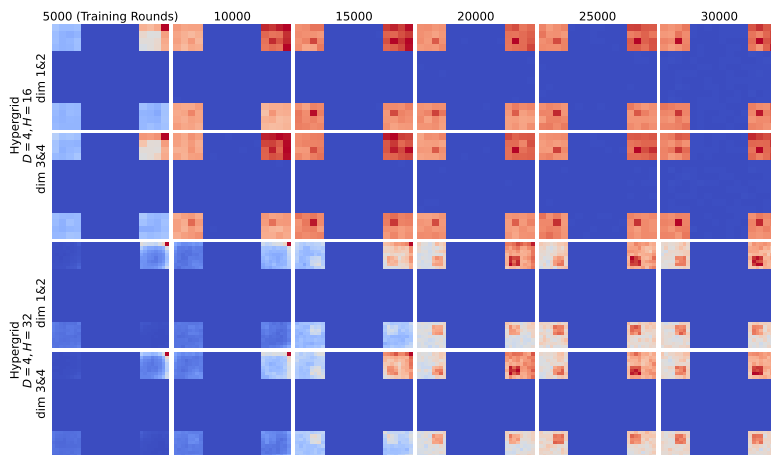


Figure 4. Learned patterns of DB. Each subfigure uses 100,000 samples.

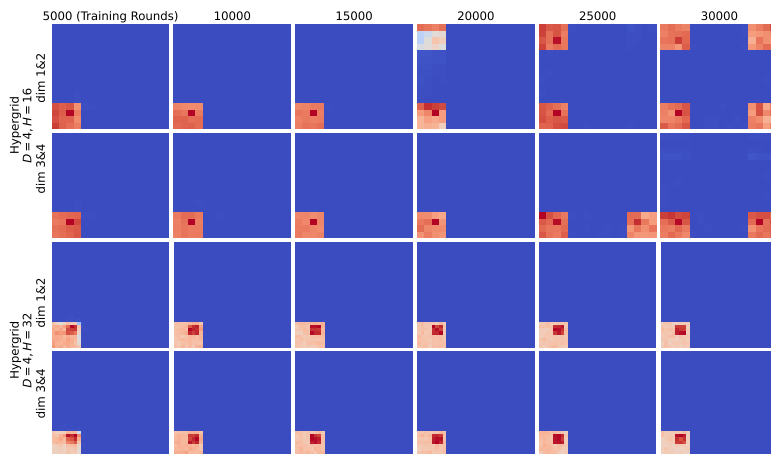


Figure 5. Learned patterns of FM. Each subfigure uses 100,000 samples.

#### D.4. Comparison Among Baselines Through the Lens of Proposition 3.10

We estimate the TV bound via Monte Carlo using Proposition 3.10. For the Hypergrid environment, we evaluate the models trained in RQ2 every 3,000 rounds, reporting the mean over five random seeds. For L14-RNA1, we use the trained model in Section D.3. For L14-RNA1, we estimate the bound every 30,000 rounds. All backward sampling for estimation uses a fixed seed of 42.

In simpler environments, we observe that FM achieves strong bounds in Hypergrid with  $H = 8$ , and AdaptiveTeacher performs well on Hypergrids by aggressively targeting high-loss trajectories. However, explicitly minimizing error on both forward and backward trajectories leads to substantially faster bound reduction.

We also note that even small sample sizes ( $N = 10$ ) prove effective for estimating TV bounds in simpler tasks. In L14-RNA1, larger sample sizes produce more stable estimates.

In this setting, meaningful TV bounds are achieved only by methods that both aggressively search for new modes and explicitly minimize errors on both sides (forward and backward).

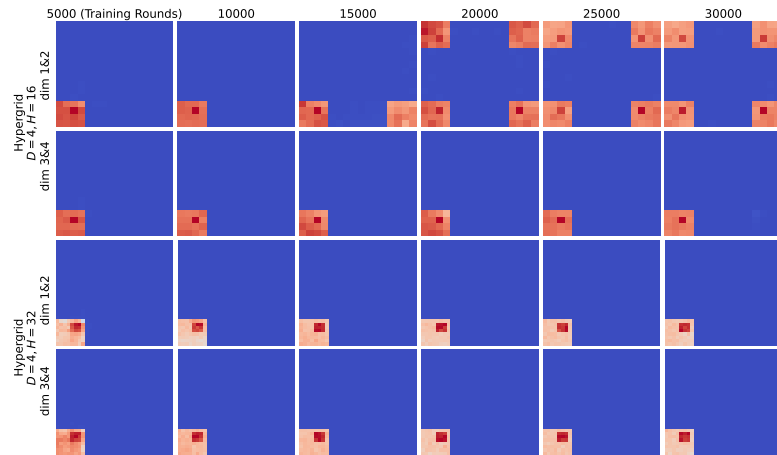


Figure 6. Learned patterns of TB. Each subfigure uses 100,000 samples.

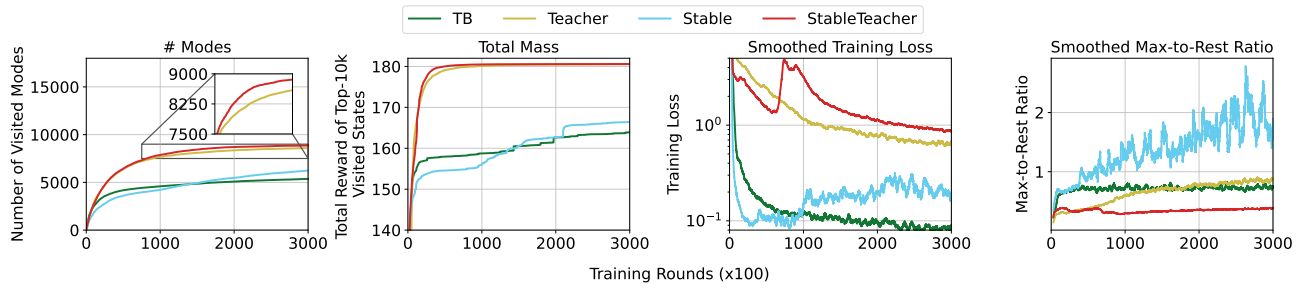


Figure 7. Extended Experiment Results for L1-RNA14.

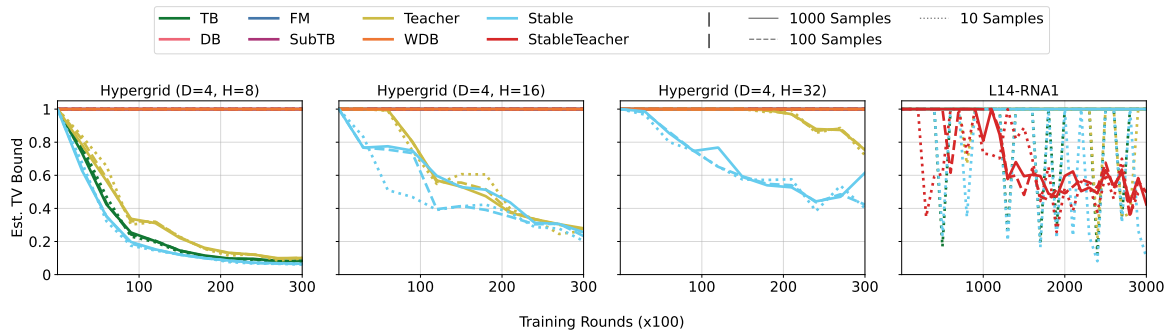


Figure 8. Evolution of TV Bounds estimated from Theorem 3.10. Here for L14-RNA1 evaluation uses the  $\mathcal{X}_{sub}$  discovered by StableTeacher (which carries the largest total reward mass), whereas Figure 3 uses  $\mathcal{X}_{sub}$  generated by standard Stable GFlowNets.